CALIBRATION OF A MULTI-COMPONENT MICRO-FORCE BALANCE SYSTEM FOR WIND TUNNEL MODELS

Semiannual Status Report

on

NASA Grant NGR 47-005-026

Submitted by Co-Principal Investigators:

Dr. James W. Moore

Dr. Eugene S. Mc Vey

and

William Thomas Mason III

Research Laboratories for the Engineering Sciences

University of Virginia

Charlottesville

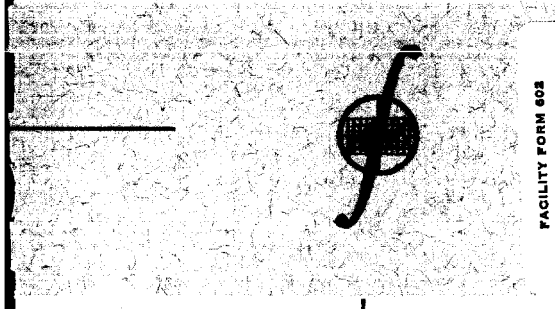

Report No. EME-4029-103A-66U

July 1966

CALIBRATION OF A MULTI-COMPONENT MICRO-FORCE BALANCE SYSTEM FOR WIND TUNNEL MODELS

Semiannual Status Report

on

NASA Grant NGR 47-005-026

Submitted by Co-Principal Investigators:

Dr. James W. Moore

Dr. Eugene S. McVey

and

William Thomas Mason III

RESEARCH LABORATORIES FOR THE ENGINEERING SCIENCES

SCHOOL OF ENGINEERING AND APPLIED SCIENCE

UNIVERSITY OF VIRGINIA

CHARLOTTESVILLE, VIRGINIA

Report No. EME-4029-103A-66U

July 1966

Copy No. _____

ABSTRACT

This thesis deals with the calibration of a multicomponent, microforce measurement system suitable for wind tunnel model testing. The system is designed to measure two orthogonal forces within a 0-0.5# range and a moment in the plane of these forces within the 0-0.2 inch pound range.

A calibration equation was developed for each measurement channel to describe the output signal of that channel as a function of the input forces and moment. These equations are composed of the main component signal plus any effects due to cross coupling between measurement channels.

A suitable loading method was developed to evaluate the coefficients of these calibration equations.

Results indicated that the cross coupling effects between measurement channels were less than one percent and that the force measurement system is suitable for wind tunnel model testing.

TABLE OF CONTENTS

CHAPTER PAGE

CHAPTER PAGE

LIST OF FIGURES

FIGURE PAGE

LIST OF TABLES

LIST OF SYMBOLS

a	Horizontal component of string force device, inches
b	Vertical component of string force device, inches
c	Horizontal distance, inches
D	Drag force, pounds
D_0	Uncorrected drag force, pounds
h	Heighth, inches
K_{ij}	General coefficient relating θ_i to ϕ_j
k_{DD}	Coefficient relating drag force input to drag channel output
k_{DL}	Coefficient relating lift force input to drag channel output
k_{DM}	Coefficient relating pitch moment input to drag channel output
L	Lift force, pounds
L_0	Uncorrected lift force, pounds
M	Pitch moment, inch-pounds
M_0	Uncorrected pitch moment, inch-pounds
mv	Millivolts
n	Total number of readout channels
P	General horizontal calibration force, pounds
p	Total number of inputs to a system
R	Magnitude ratio
W	Weight, pounds
X	Coordinate for ± lift axis
Z	Coordinate for ± drag axis
α	Angle of inclination of load application fiber
β	Angle of elevation on string force device
δ	Offset of sting at bottom, inches
θ_i	General output of a readout channel
θ_D	Readout signal of drag channel, millivolts
θ_L	Readout signal of lift channel, millivolts
θ_M	Readout signal of pitch channel, millivolts
ϕ_j	General input to measurement system
ψ	Horizontal angle in X-Z plane

CHAPTER I
INTRODUCTION

This thesis deals with the development of a technique and the necessary equipment for the calibration of a multi-component, micro force measurement system suitable for wind tunnel model testing.

BACKGROUND

In the past, with wind tunnel test models relatively large, force measurements were made with strain gage instrumented structures. The models were mounted on structural members, internal to the model, which were deflected when loaded with the aerodynamic forces. The models were large and the air stream relatively dense so that the aerodynamic forces were large enough to be accurately measured with conventional strain gage techniques.

Recent advances in aerospace research have brough about a need for more precise methods of wind tunnel model evaluation. In particular, with wind tunnel models becoming lighter and smaller as tunnel speeds and temperatures increase, more sensitive force measurement systems are needed to measure the resultant smaller aerodynamic model loads.

Research dealing with one possible system for the measurement of small forces is presently being conducted as a joint effort between the Electrical and Mechanical Engineering Departments of the University of Virginia. This system, shown in Figure I is to be used for testing small aerodynamic models in an arc heated, hypersonic wind tunnel. This system is a null balance type in which the unknown force is opposed by a known force. The research is sponsored by the Force Measurement Group of NASA at Langley, Virginia.

Previous work on this system was involved with the design and fabrication of a frictionless air bearing support for the system[1] and the

[1] David A. Hicks, "Design and Development of a Gas-Supported Hydrostatic Thrust Bearing" (unpublished Masters' thesis, The University of Virginia, Charlottesville, 1965).

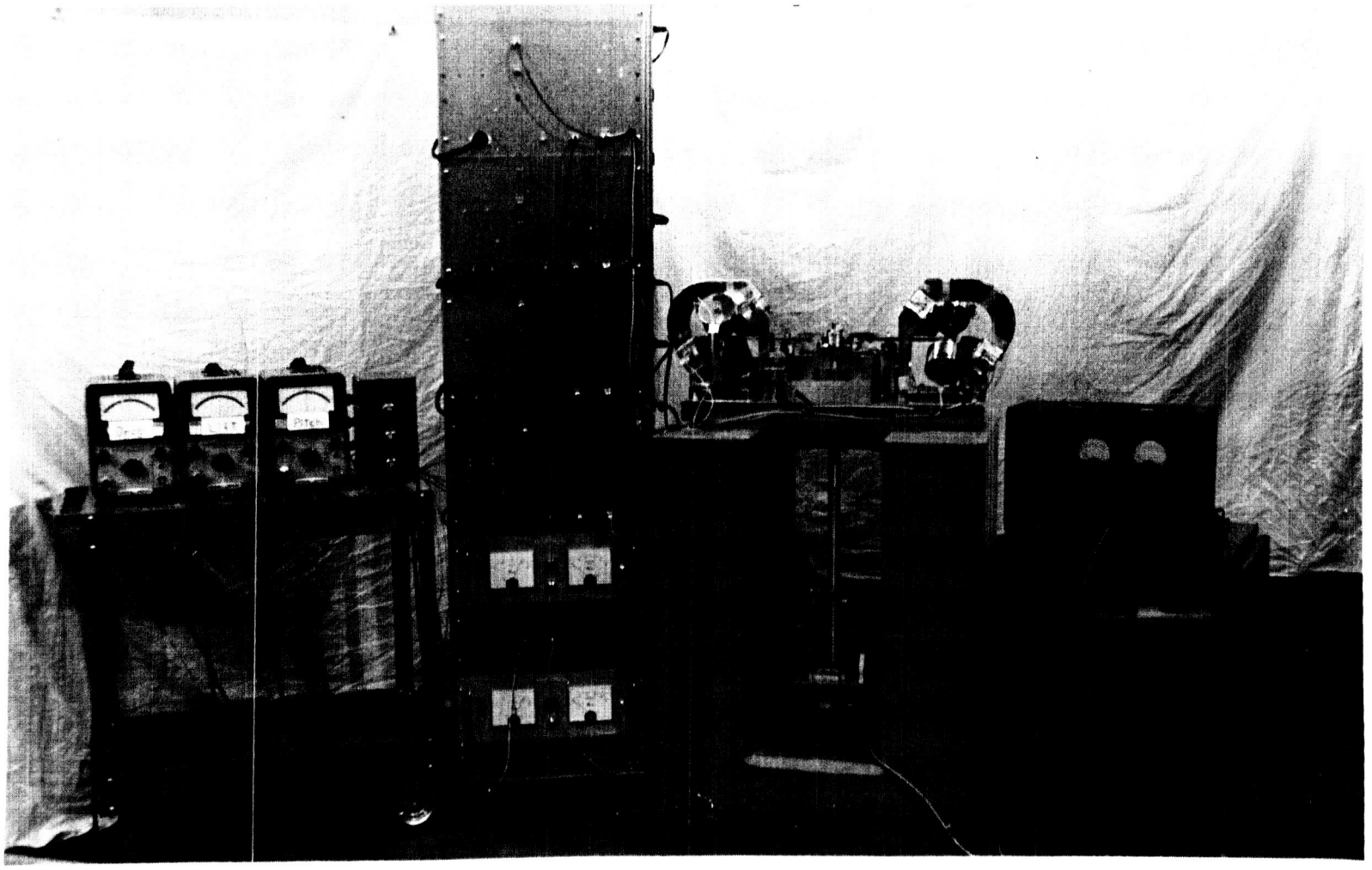

FIGURE 1 OVERALL VIEW OF FORCE MOVEMENT SYSTEM

development of an automatic control system to provide the restoring forces to balance the unknown forces[2].

As with any piece of instrumentation, a force measurement system is only as good as the final calibration procedure performed on it. The calibration procedure for any piece of instrumentation equipment serves three main purposes. First, and most important, it determines the measuring characteristics of the equipment such as input-output ratio, repeatability of readings, hysteresis effects, and precision. The calibration procedure also provides test data which can be used to check the instrument's performance with that predicted by theoretical analysis. And finally, the test data obtained from the calibration procedure will often suggest needed or desired improvements in the measurement system.

SCOPE

A set of calibration equations are developed which describe the input-output relations for the system as a series of terms consisting of input forces and appropriate coefficients. The design and fabrication of a calibration balance suitable for applying small, precise calibration loads is covered. The use of this balance to determine the coefficients of the calibration equations is discussed as well as an analysis of the output signals of the system. The linearity, hysteresis, repeatability, and sensitivity of the system are determined to determine the suitability of the system for wind tunnel model testing.

---

[2]Karl C. Henderson, "A Control System for the Measurement of Multi-Component, Micro-Forces on a Wind Tunnel Model" (unpublished Masters' thesis, The University of Virginia, Charlottesville, 1966).

CHAPTER II
DISCUSSION OF FORCE MEASUREMENT SYSTEM

The force measurement system presently being developed for wind tunnel model evaluation is a null-balance type in which the unknown force is balanced by a known force. This system employs an input arm supported by an air bearing and positioned by a closed loop servo-mechanism system.

Figure 2 illustrates the basic operating principles of this system. The model is mounted on an input arm (sting) projecting into the wind tunnel test section. This sting is supported by an air bearing with upper and lower bearing areas so that the sting is free to translate and rotate within a horizontal plane but is constrained in all other directions. The sting is held in an equilibrum position by three independent closed loop servo systems, each consisting of a displacement transducer, amplifier, and linear force motor.

A force on the model will produce a displacement of the sting which is sensed by an LVDT displacement transducer. This signal is amplified and fed to the linear force motor to produce a force to restore the sting to equilibrum position. Since the air bearing is approximately frictionless[3], the restoring force is equal in magnitude to the original unknown force. The restoring force of the motor will be proportional to the motor coil current and therefore the motor coil current will be proportional to the unknown force. Thus, after the system has been properly calibrated, the unknown force may be determined by measuring the motor coil current.

The above analysis is for the steady state case where initial transients have died out. This is not a rigid restriction as wind tunnel run times will be on the order of thirty to sixty seconds while system response is on the order of 200 milliseconds.

The present system is designed to measure two orthogonal components of force in a horizontal plane as well as a moment within this plane. Figure 3 shows the orientation of the three servo systems with respect to

---

[3]Hicks, op. cit., p. 54.

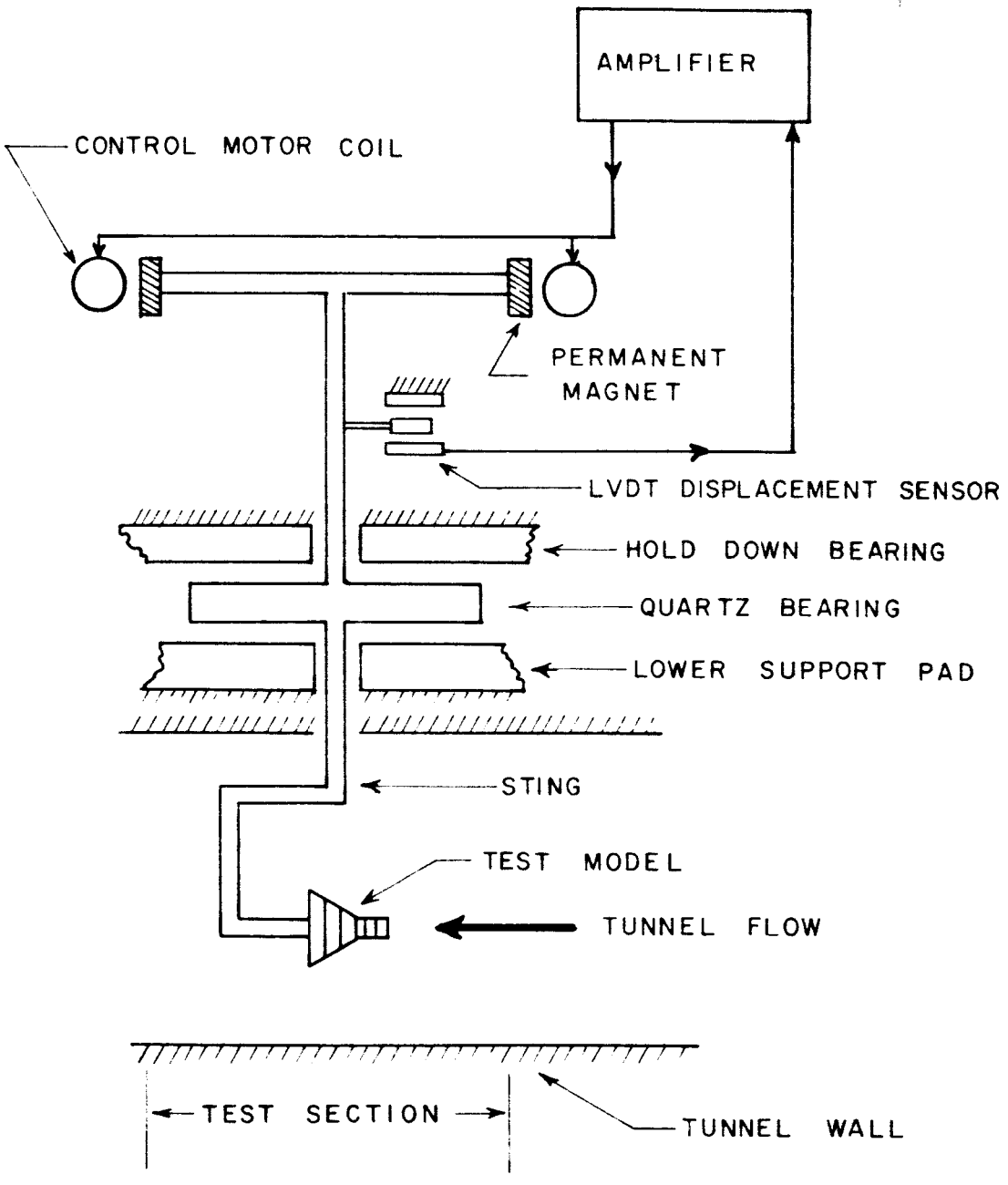

FIGURE 2 SIDE VIEW OF FORCE MEASUREMENT SYSTEM (SINGLE CONTROL LOOP SHOWN)

the model to be tested. Sensor X_{12} detects displacements in ± X direction and controls current in coil pairs X_1 and X_2 to keep the system at the equilibrium position with respect to X. Current in coil pair Z_1 is controlled by sensor Z_1 and current in coil pair Z_2 is controlled by sensor Z_2. A pure Z translation will produce equal signals in sensors Z_1 and Z_2 with resultant equal restoring forces in coil pairs Z_1 and Z_2. A positive pitching moment M will produce a positive displacement at the Z_2 sensor and a negative displacement at the Z_1 sensor. These displacements will produce signals at sensors Z_1 and Z_2 which in turn will produce a positive current in the Z_2 coil pair and a negative current in the Z_1 coil pair. These currents will drive the system back to the original equilibrium position. With all three servo systems working simultaneously, the model-sting system will be held in equilibrium in the X-Z plane. The sum of the currents in coil pairs X_1 and X_2 is proportional to the drag force D, the sum of the currents in coil pairs Z_1 and Z_2 is proportional to the lift force L and the difference between the currents in coil pairs Z_1 and Z_2 is proportional to the pitching moment M. Thus, the lift force L, drag force D and pitching moment M due to aerodynamic forces on the model can be determined from the currents in coil pairs X_1, X_2 and Z_1, Z_2.

The actual readout signal is a voltage developed across a readout resistor by the motor coil current. The drag output signal is the sum of voltage in readout resistors of motor coils X_1 and X_2. The lift output signal is the sum of voltages across readout resistors of motor coil Z_1 and Z_2. Solid state operational amplifiers are used to provide the necessary high input impedance of the summer and subtractor circuits.

The system has been designed to measure drag and lift forces within the range of 0-0.5 pounds and pitching moments within the range of 0-2.0 inch-pounds. The above load capacities were split into two measurement ranges to provide measurement ranges of 0-0.5# and 0-0.5# on drag and lift channels and pitch channel ranges of 0-0.2 inch pound and 0-2.0 inch pound. To provide the necessary readout precision, a two-position range switch is used on each of the three readout channels. This switch selects between two readout resistors which have relative

magnitude valves of 1 and 10. This provides approximately equal output signals for the 0-0.5# and 0-0.05# ranges. The readout box has a full scale output of approximately 1000 mv for both of the ranges on the lift and drag channels and approximately 350 mv for the two pitch channel ranges. Figure 4 is a closeup view of the control motor coils and air bearing support. The permanent magnet of the X_2 and Z_2 control motors can be seen in the center of the four coils at the right side of the system.

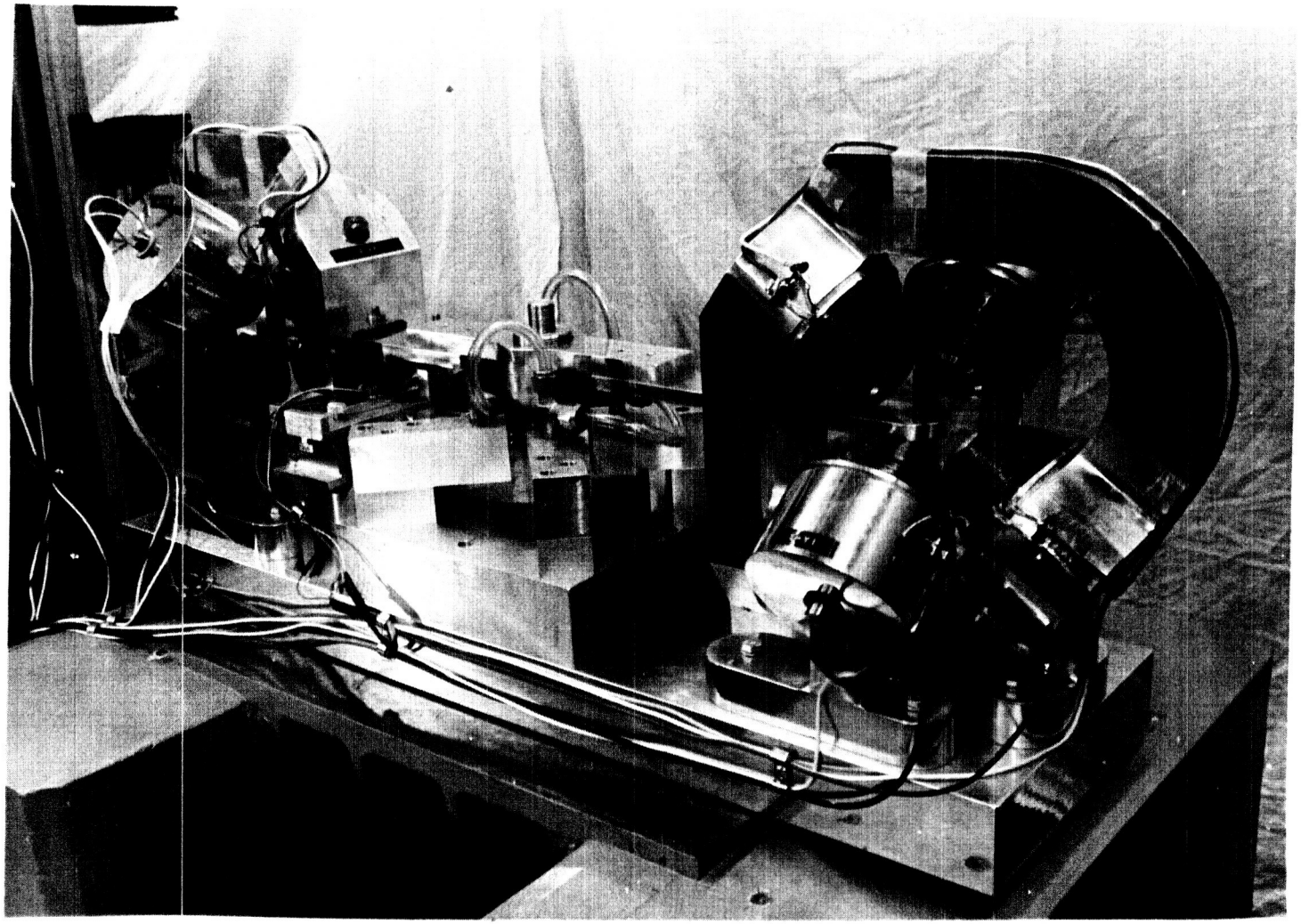

FIGURE 4 CLOSEUP OF CONTROL MOTORS AND AIR BEARING

CHAPTER III
DISCUSSION OF CALIBRATION PROCEDURE

The linear force motors in this system were designed to produce a pure single component force with no interaction effects. That is, a current in the Z_1 coil pair should theoretically produce only a pure Z directed force. Also, current in coil pair X_1 should theoretically produce a force in the pure X direction regardless of the current in coil pair Z_1. In actual practice these pure uncoupled forces may not exist as predicted.

In addition to motor cross coupling there may be some cross coupling due to the orthogonality of the sensor mountings. As can be seen in Figure 3, a motion of the sting in a pure X direction will produce a radial motion of the cores of sensors Z_1 and Z_2 relative to their transformer coils. Similarly, a pure Z displacement will produce a radial motion of the core of X_{12} sensor relative to its transformer coil. In general, the radial sensitivity of a LVDT lies within the range of 0.1 to 1% of its axial sensitivity[4] and although this value is small, there will still be a finite amount of cross coupling due to this effect.

The calibration procedure must prove or disprove the existence of these cross coupling effects and must be capable of determining their magnitudes. The calibration of this system was limited to the determination of two types of cross coupling effects. These two types are direct cross coupling and cross product coupling. Direct cross coupling occurs when the readout signal of one unloaded channel is affected by a loading in another channel. An example of this would occur when pure lift is applied to the system and the drag readout channel indicates an applied drag even though none was applied. Cross product coupling produces an effect which is proportional to the product of the loads on two separate channels. An example of this would occur when the readout on the drag channel due to an applied drag would be affected by a load applied in the pure lift direction.

---

[4]Kurt S. Lion, Instrumentation in Scientific Research. New York: McGraw Hill Book Company, 1959) p. 51.

DEVELOPMENT OF CALIBRATION EQUATION

The effect of these cross coupling phenomena on the force measurement system can be expressed by a calibration equation which relates the input to the system to the output. The determination of this equation is the purpose of a calibration procedure. For the general case, let θ_i be the output of a particular readout channel and let ϕ_j be a particular input to the system. Then $\theta_i = f(\phi_j)$ where i and j are the indices of the output and input respectively. The output for a particular channel can be expressed as a sum of terms consisting of the product of an input with a constant of proportionality. Let K_{ij} be the coefficient relating the jth input to the ith output. Then θ_i can be expressed as the following sets of equations.

$$\theta_1 = \phi_1 K_{11} + \phi_2 K_{12} + \phi_3 K_{13} + \ldots \phi_j K_{ij}$$

$$\theta_2 = \phi_1 K_{21} + \phi_2 K_{22} + \phi_3 K_{23} + \ldots \phi_j K_{2_j}$$

" " " " " "

$$\theta_i = \phi_1 K_{i1} + \phi_2 K_{i2} + \phi_3 K_{i3} + \ldots + \phi_j K_{ij}$$

or for the general case

$$\theta_i = \sum_{\substack{i=1 \\ j=1}}^{\substack{i=n \\ j=p}} \phi_j K_{ij} \qquad \text{where} \begin{cases} i = 1, 2, 3 \ldots n \\ j = 1, 2, 3 \ldots p \end{cases}$$

where n is the total number of readout channels and p is the total number of inputs which affect the measurement system. For a force measurement system the ϕ_j would be the input forces plus any other variables such as temperature, time, etc., which affect the output. These inputs are not restricted to linear terms and may in fact be second or third order interactions.

APPLICATION TO FORCE MEASUREMENT SYSTEM

For the system to be calibrated, there are three readout channels: one for drag D, one for lift L, and one for pitching moment M. We may write the following calibration equation for the Drag channel.

$$\theta_D = DK_{DD} + D^2K_{DD^2} + LK_{DL} + L^2K_{DL^2} + MK_{DM} + M^2K_{DM^2} +$$

$$LDK_{DLD} + LMK_{DLM} + DMK_{DDM}$$

where
- θ_D = output at drag channel readout
- D = Applied drag
- L = Applied lift
- M = Applied pitch
- D^2, L^2, M^2, are second order interaction inputs.
- LD, LM, DM, are cross product interaction inputs.

The above equation can be rearranged to make it more useful as a means of determining the unknown force, D. Dividing both sides of the equation by K_{DD} and moving all terms on the right side, except D, to the left side gives the following:

$$D = \frac{\theta D}{K_{DD}} - \left[\frac{D^2K_{DD^2}}{K_{DD}} + \frac{LK_{DL}}{K_{DD}} + \frac{L^2K_{DL^2}}{K_{DD}} \ldots + \frac{DMK_{DDM}}{K_{DD}} \right]$$

Redefining the coefficients gives

$$D = \theta_D k_{DD} - [\, D^2k_{DD^2} + Lk_{DL} + L^2k_{DL^2} + \ldots DMk_{DDM} \,]$$

$\therefore$ D = Primary Term - Interaction Terms

Similiar equations can be written for the lift and pitch readout channels.

The primary and interaction coefficients are evaluated by loading the force measurement system with both single forces and combinations of forces[5].

DETERMINATION OF UNKNOWN FORCES

The above equation plus the appropriate equations for lift and pitch are used to carry out an iteration process to determine the real drag, lift, and pitch loadings. For a first approximation we determine $D_0 = \theta_D k_{DD}$, $L_0 = \theta_L k_{LL}$, and $M_0 = \theta_M k_{MM}$ and insert these values into the calibration equation to get

$$D_1 = D_0 - [D_0{}^2 k_{DD^2} + L_0 k_{DL} + \ldots \text{ etc.}]$$

$$L_1 = L_0 - [L_0{}^2 k_{LL^2} + D_0 k_{LD} + \ldots \text{ etc.}]$$

$$M_1 = M_0 - [M_0{}^2 k_{MM^2} + D_0 k_{MD} + \ldots \text{ etc.}]$$

This gives us more accurate values of drag, lift and pitch and these values are substituted back into the equation to give:

$$D_2 = D_0 - [D_1{}^2 k_{DD^2} + \ldots \text{ etc.}]$$

$$L_2 = L_0 - [L_1{}^2 k_{LL^2} + \ldots \text{ etc.}]$$

$$M_2 = M_0 - [M_1{}^2 k_{MM^2} + \ldots \text{ etc.}]$$

This iterative procedure is continued until the difference between iterations reaches some preassigned value[6].

---

[5]J. F. Guarino, "Calibration and Evaluation of Multicomponent Strain-Gage Balances" (a paper prepared for presentation to the N. A. S. A. interlaboratory force measurements group meeting held at J. P. L. on April 16 and 17, 1964) p. 4 (Mimeographed).

[6]Ibid., p. 11.

CHAPTER IV
DESIGN AND FABRICATION OF CALIBRATION EQUIPMENT

Calibration of the system required that a precisely known horizontal force be applied to the sting so that it closely approximated the aerodynamic loading of a model in the wind tunnel test section. In order to meet this requirement, the following factors were considered to be important in the selection of a suitable loading device.

SIZE AND LOCATION

The force measurement system had already been mounted on a test pad as shown in Figure 5. Thus, it was necessary that any loading device fit within the support walls of the test pad. It was also considered desirable for the calibration force to be applied at the same location on the sting as a model would be located.

MOBILITY OF CALIBRATION FORCE

It was considered necessary to be able to rotate this calibration force around the center of the force measurement system. This would allow an accurate determination of the system axes and would provide a check on the orthogonality of the lift and drag measurement channels.

EASE OF OPERATION OF CALIBRATION EQUIPMENT

A calibration set up was desired which would provide the most accurate and easiest to use force application method. It was decided that the most direct way to obtain a force was to use standard calibrated weights such as analytical balance weights of high precision which are readily obtained. This would prevent the need for an intermediate calibration step such as would be required for a calibration force obtained from a spring deflected through a measured displacement.

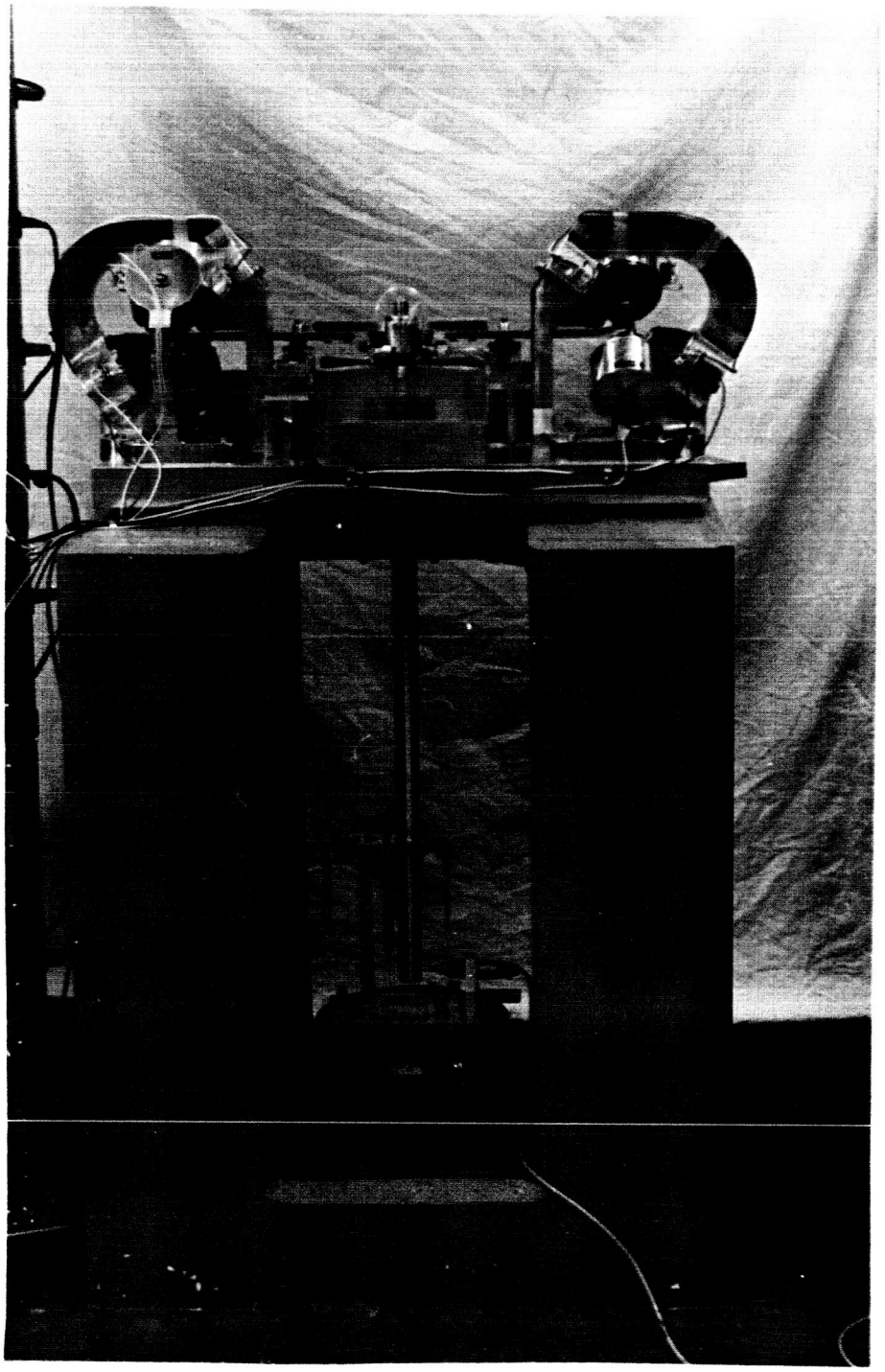

FIGURE 5 SYSTEM MOUNTED ON TEST PAD

The method finally selected for force application was an equal arm balance with a vertical force beam as shown in Figure 6. A balance such as this could be made to fit within the walls of the test pad and at the same time would provide the required mobility and ease of operation. A balance with maximum sensitivity and repeatability was desired. To achieve this end, the following theoretical investigation of balance performance was carried out.

ANALYSIS OF EQUAL ARM BALANCE PERFORMANCE

Consider a general equal arm balance as shown in Figure 7 with the terms defined as follows:

- w = weight of balance (without pans)
- W = Initial weight plus pan weight
- ΔW = Incremental weight loaded to produce θ
- θ = Angle turned due to ΔW
- ℓ = length of upper beam from piviot pt. to pan loading pt.
- 0 = Point of suspension of balance
- D = location of center of gravity
- A & B = points of attachement for balance pans
- X = Distance between "0" and Line joining A & B
- Y_0 = Distance between "0" and "D"

Assume an incremental weight ΔW has been loaded in the left pan to produce a tilting of the balance.

Equating clockwise and counter-clockwise moments gives:

$$(W + \Delta W)(\ell \cos\theta - X \sin\theta) + w(Y_0 \sin\theta) = W(\ell \cos\theta - X \sin\theta)$$

Multiplying through and simplifying gives

$$2WX \sin\theta + \Delta W \ell \cos\theta + \Delta WX \sin\theta + wY_0 \sin\theta = 0.$$

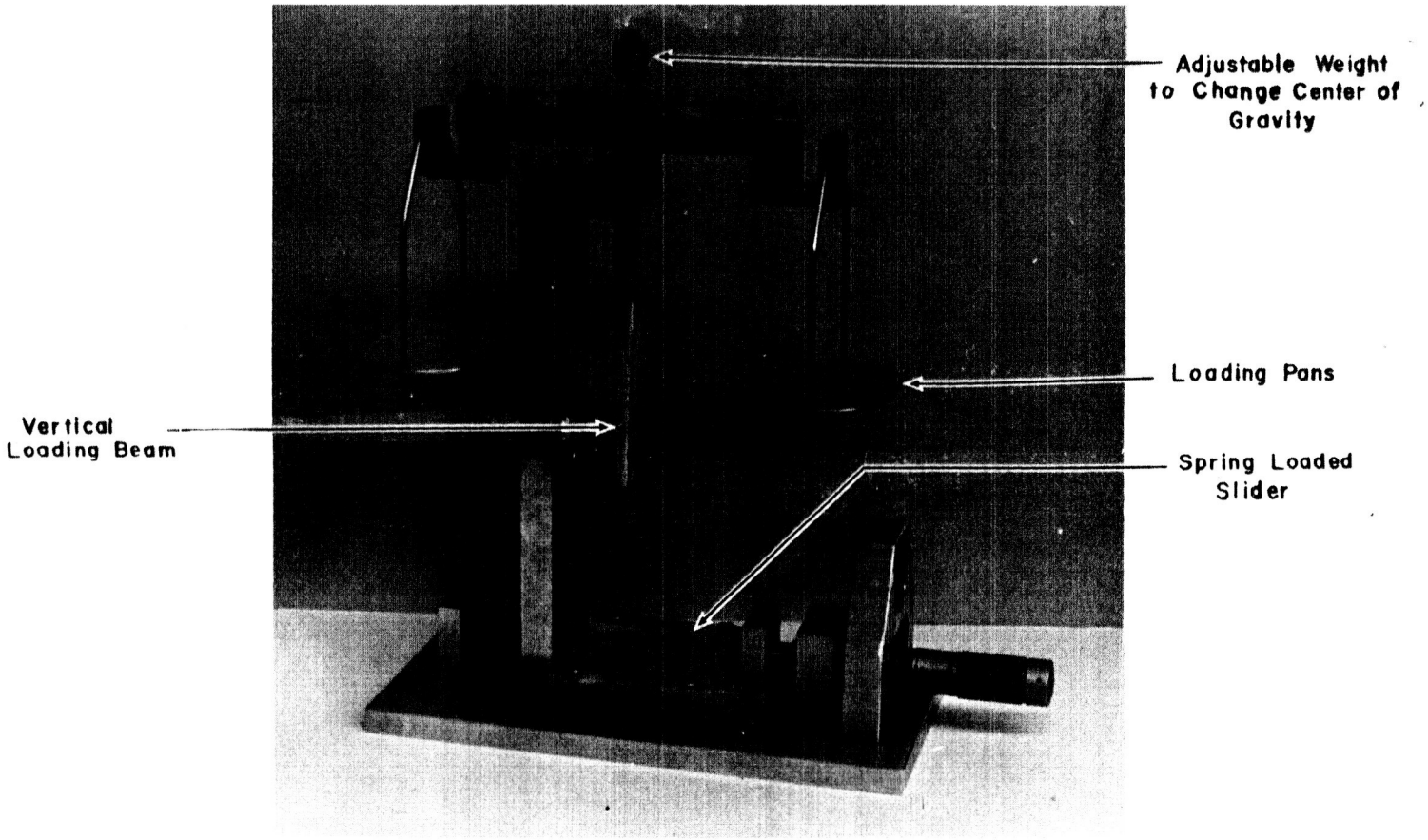

FIGURE 6 CALIBRATION BALANCE

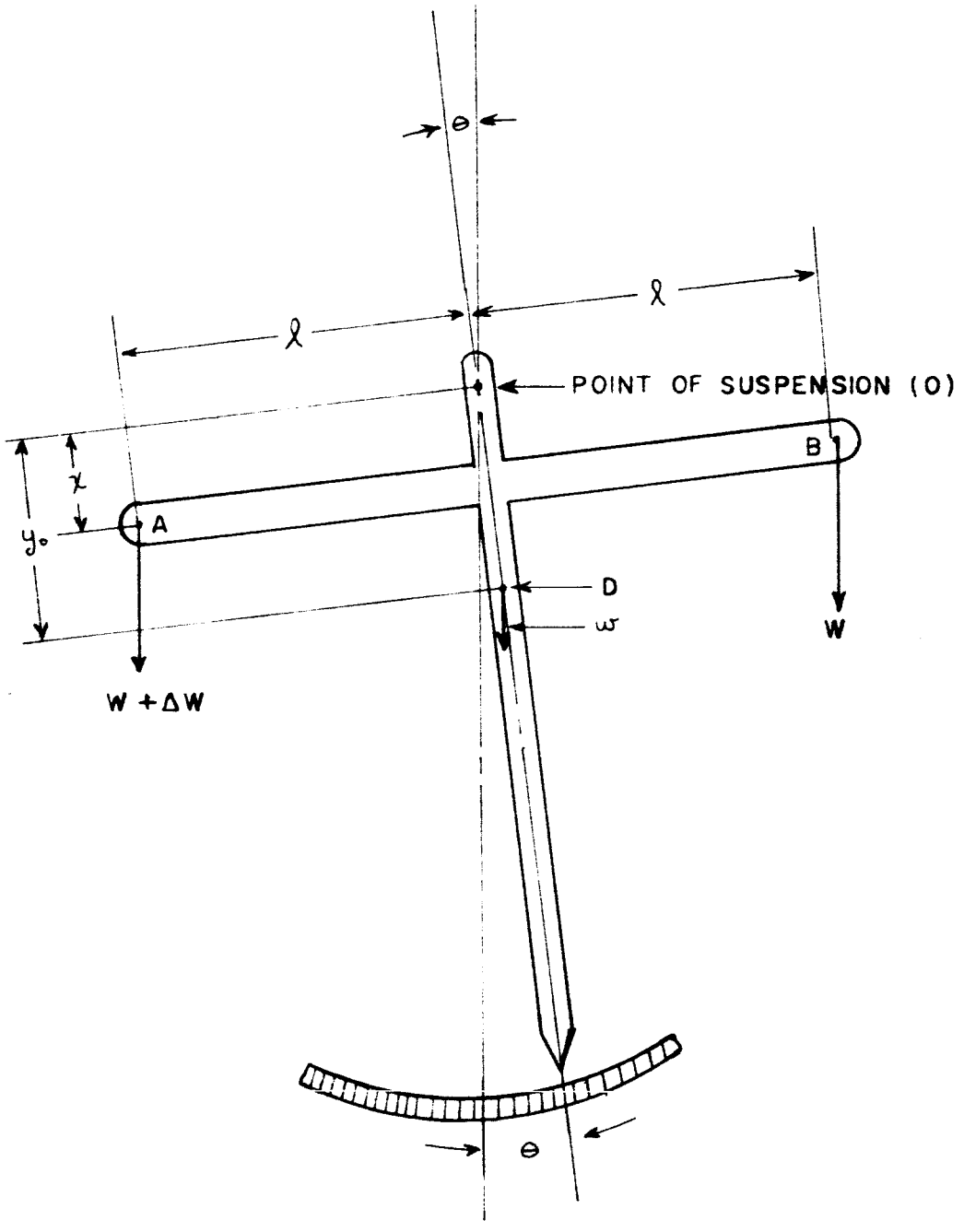

FIGURE 7 EQUAL ARM BALANCE (GENERAL)

Now, for small θ, $\sin\theta \approx \theta$ and $\cos\theta \approx 1$.

$$2WX\theta + \Delta W\ell + \Delta WX\theta + wY_0\theta = 0$$

$$(\Delta W)\ell = (2WX + \Delta WX + wY_0)$$

Rearranging gives

$$\frac{\theta}{\Delta W} = \frac{\ell}{2WX + \Delta WX + WY_0}$$

Now, the incremental weight ΔW will be small compared to the other two terms in the denominator and may be neglected. Also, by making the point of suspension ("0"), colinear with the pan loading points "A" and "B", X will be zero and thus:

$$\frac{\theta}{\Delta W} = \frac{\ell}{wY_0}$$

which is the basic sensitivity equation for the balance[7]. Now for $\frac{\theta}{\Delta W}$ to be a maximum, ℓ must be a maximum while w and Y_0 must be minimums. This means that the balance should have a very long arm of negligible weight and still be stiff enough to prevent any deflections to produce an "X" term. Obviously, these conditions are contradictory and cannot all simultaneously be met. The limiting factor is ℓ since the balance must be small enough to fit into the test section. L was set at 3" and the other dimensions were arrived at by a trial and error design process on paper. The dimensions of the various parts of the balance were adjusted so as to reduce the weight to a minimum and yet provide the necessary structural rigidity. At the same time, the relative positions of the parts were adjusted so as to make the center of gravity of the balance close to the point of suspension (i.e., make Y_0 a minimum).

---

[7]Nathan A. Cook and Ernest Rabinowicz, Physical Measurement and Analysis. Reading, Massachusetts: Addison-Wesley Publishing Company, 1963) pp. 13-14.

An adjustable weight on the top of the calibration balance was provided so that small changes in Y_0 could be effected to reduce the restoring force of the balance to a minimum. This weight, shown in Figure 6, provided a compensation for inaccuracies in machining of the parts and slight assembly tolerances. The balance was made by the Cole Tool Company of Waynesboro, Virginia and except for the knife edges, was made of aluminum to reduce component weights and avoid extraneous effects on the magnetic fields of the control motors. The knife edges were made of steel and where ground and hardened to reduce friction. Mr. Schenkel of the RLES staff did a careful lapping job on the matched pairs of knife edges to further reduce the friction.

The balance was mounted on a spring loaded slider assembly as shown in Figure 6 so that it could be properly positioned with respect to the sting. This slider was positioned with a micrometer and allowed any deflection of the sting to be easily compensated for, so as to maintain the balance at a level position.

STRING FORCE DEVICES

Two force application devices were borrowed from the Force Measurement Group of NASA at Langley, Virginia to apply supplementary loads to the system during calibration. These were used to apply pitch to the system as well as secondary lift loads for cross coupling determination. In addition, they were used to apply the lift and drag loads for the lower (0.05#) range calibration.

As can be seen in Figure 8 these devices are used to position a weight suspended on a string so that the horizontal component of force is a given fraction of the suspended weight. The horizontal force component is P where:

$$P = W \operatorname{cotan} \beta = W\left(\frac{a}{b}\right)$$

The a/b ratio has been set at $\frac{1}{2}$ so that the horizontal calibration force P is equal to one-half the suspended weight W. Since the effects of

contact friction and string bending stiffness of a thin, static, hanging string are negligible, the accuracy of the horizontal force of this device is only limited by the precision of the weights and the precision of the measurement of a and b.

BALANCE PERFORMANCE CHECK

The ultimate limit on the precision of the balance was found to be the friction of the knife edge supports. Even after careful lapping, a small amount of hysteresis producing friction was present and a test was devised to determine the magnitude of its effects. The balance was set up as shown in Figure 9 so that it could easily be loaded with a horizontal force from the string force device. The balance pan was loaded with a weight sufficient to balance the horizontal load of the string force device. Then, small weights were added to the balance pan until breakaway from equilibrium occurred. This incremental load was considered the force necessary to overcome static knife edge friction for that particular balance load. This incremental weight was expressed as a percentage of the balance load and a plot of the results of this test is given in Figure 10. It can be seen that the error in the applied calibration force due to knife edge friction is less than 0.2% for calibration forces greater than 0.05#.

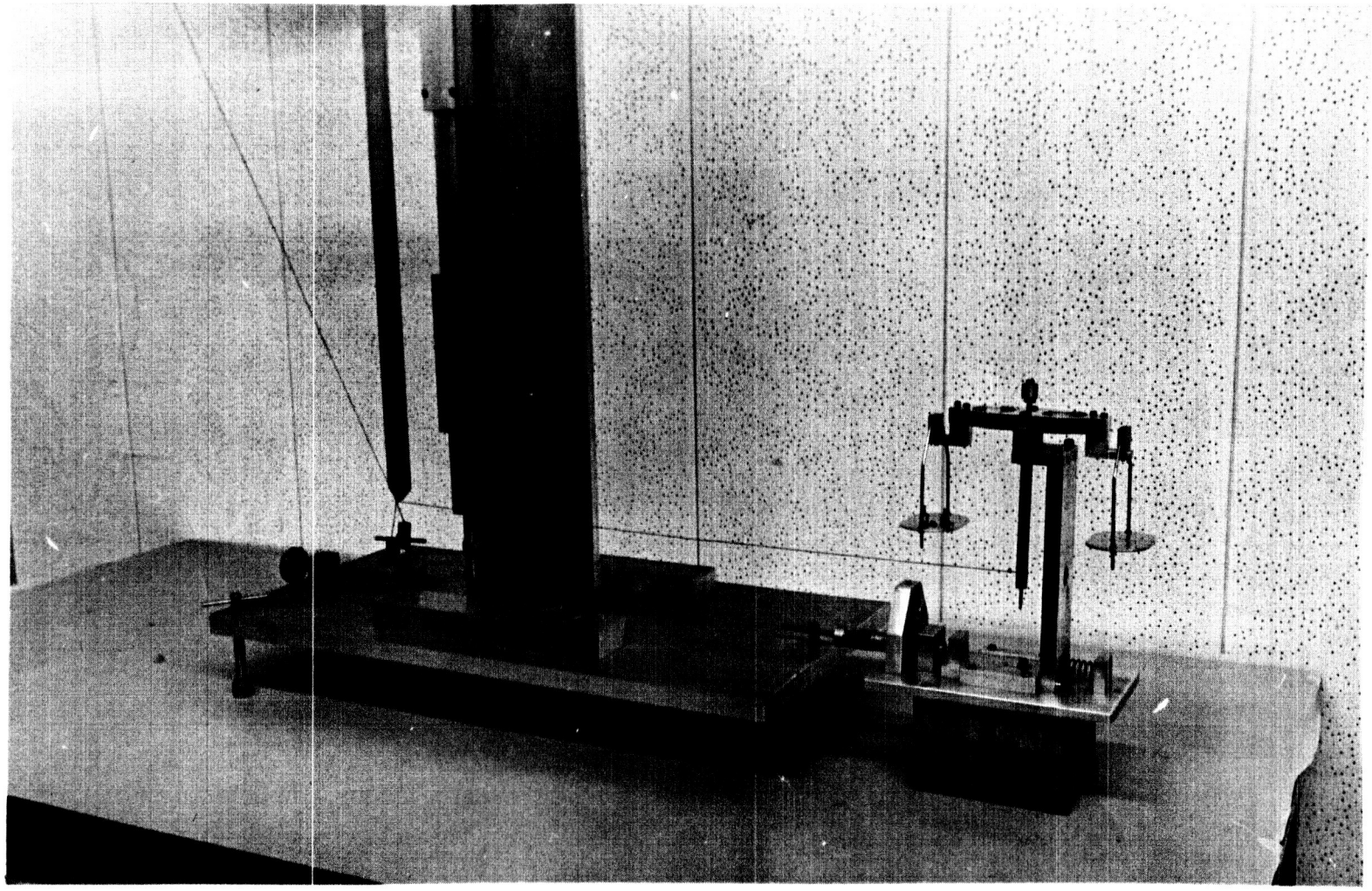

FIGURE 9 SETUP TO EVALUATE BALANCE KNIFE EDGE FRICTION

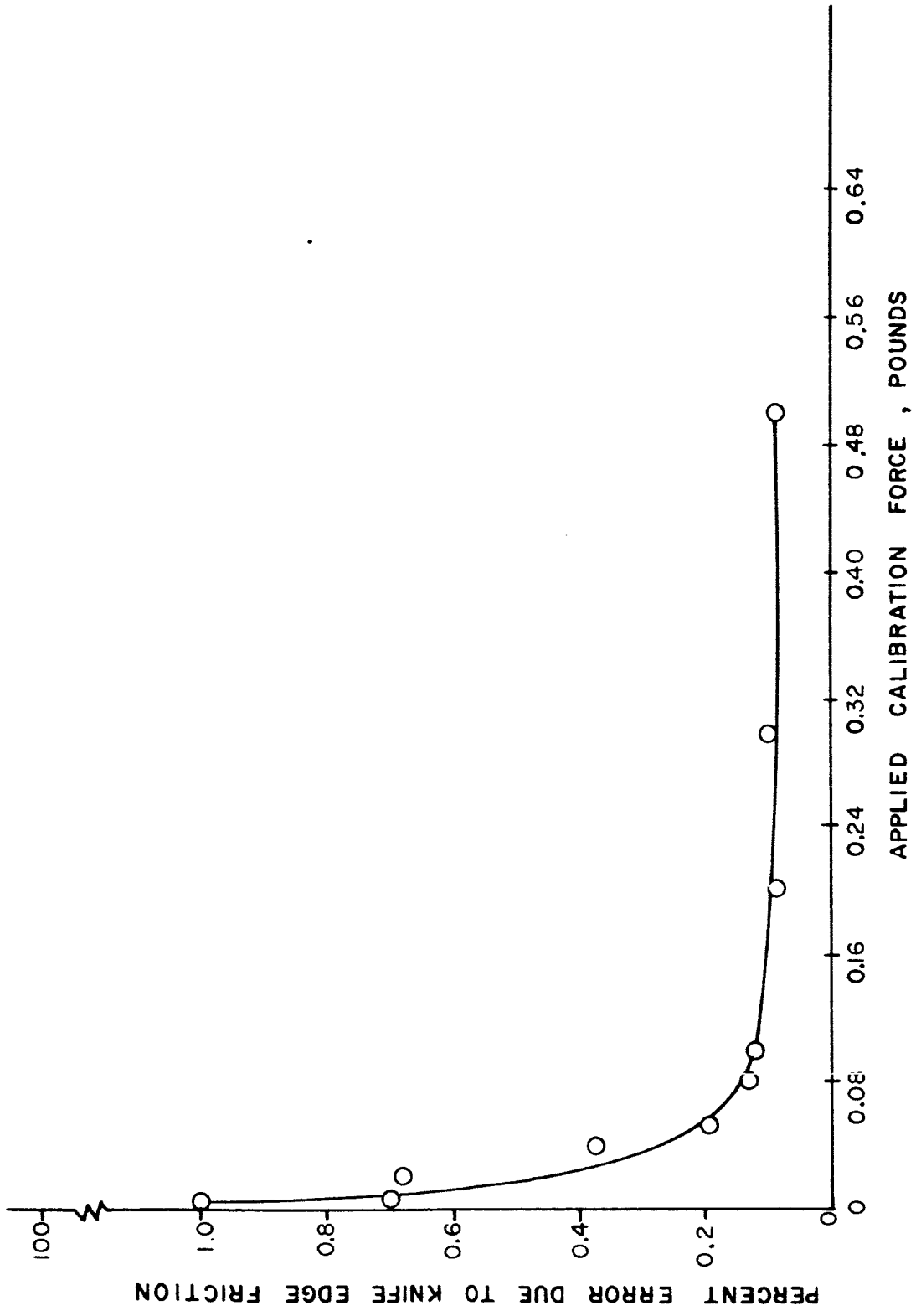

FIGURE 10 KNIFE EDGE FRICTION EFFECTS

CHAPTER V
ACTUAL CALIBRATION OF SYSTEM

DETERMINATION OF SYSTEM MEASUREMENT AXES

Before any calibration of the system was begun, a test was made to determine the true coordinate axes for the lift and drag directions. Theoretically, the lift and drag components should be orthogonal and should coincide with the actual physical system axes. The loading balance was set up on a machinist's rotary table as shown in Figure 11 so that the horizontal angle of loading could be easily varied. As an initial point of reference, the ± drag axis was assumed to run through the centers of the two control motor coil pairs X_1 and X_2.

A positive drag load of 0.323 pounds (65% of fullscale value) was then applied to the sting at one degree intervals for ±15° from the assumed zero axes. For each load application, the lift channel output was read and recorded. This procedure was repeated for three separate trials. A plot of the average lift channel output -vs- horizontal angle ψ was made and the results are shown in Figure 12. Assuming no cross coupling, the true coordinate axes for the ± drag component should be at an angle ψ where the lift signal output is zero. The lift channel output will be more sensitive to changes in the angle of drag loading ψ, than will the drag channel output. The reason for this is shown in Figure 16. It can be seen that the net drag applied to the system is P cos ψ while the net applied lift is P sin ψ. For $\psi = 0$, the applied drag is P cos (0°) = P and the lift is P sin (0°) = 0. Now, let ψ be a small, non-zero angle such as 1°. The applied drag is now P cos (1°) = P(0.9998) and the lift is P sin (1°) = P(0.0175). The net change in the readout channels are $(\frac{1-0.9998}{1}) \times 100 = 0.02\%$ for the drag channel and $(\frac{1-0.0175}{1}) \times 100 = 1.75\%$ of full scale for the lift channel output. A one percent change in the drag channel output signal requires an eight degree change in ψ while a one percent change in the lift channel output signal only requires a 0° 35' change in ψ. Thus the readout channel orthogonal to the one being loaded gives the most sensitive check on the loading angle.

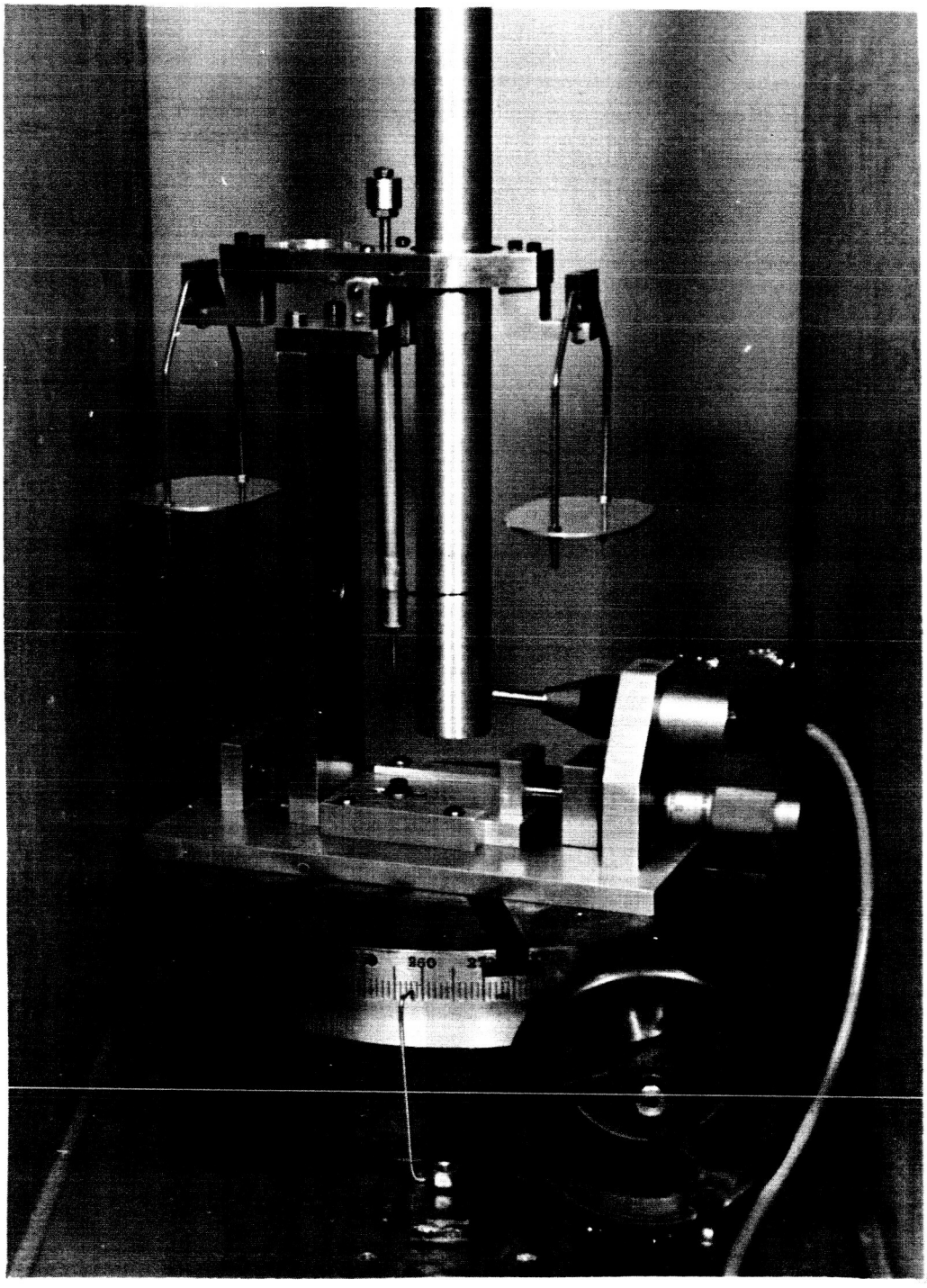

FIGURE 11 BALANCE MOUNTED ON ROTARY TABLE

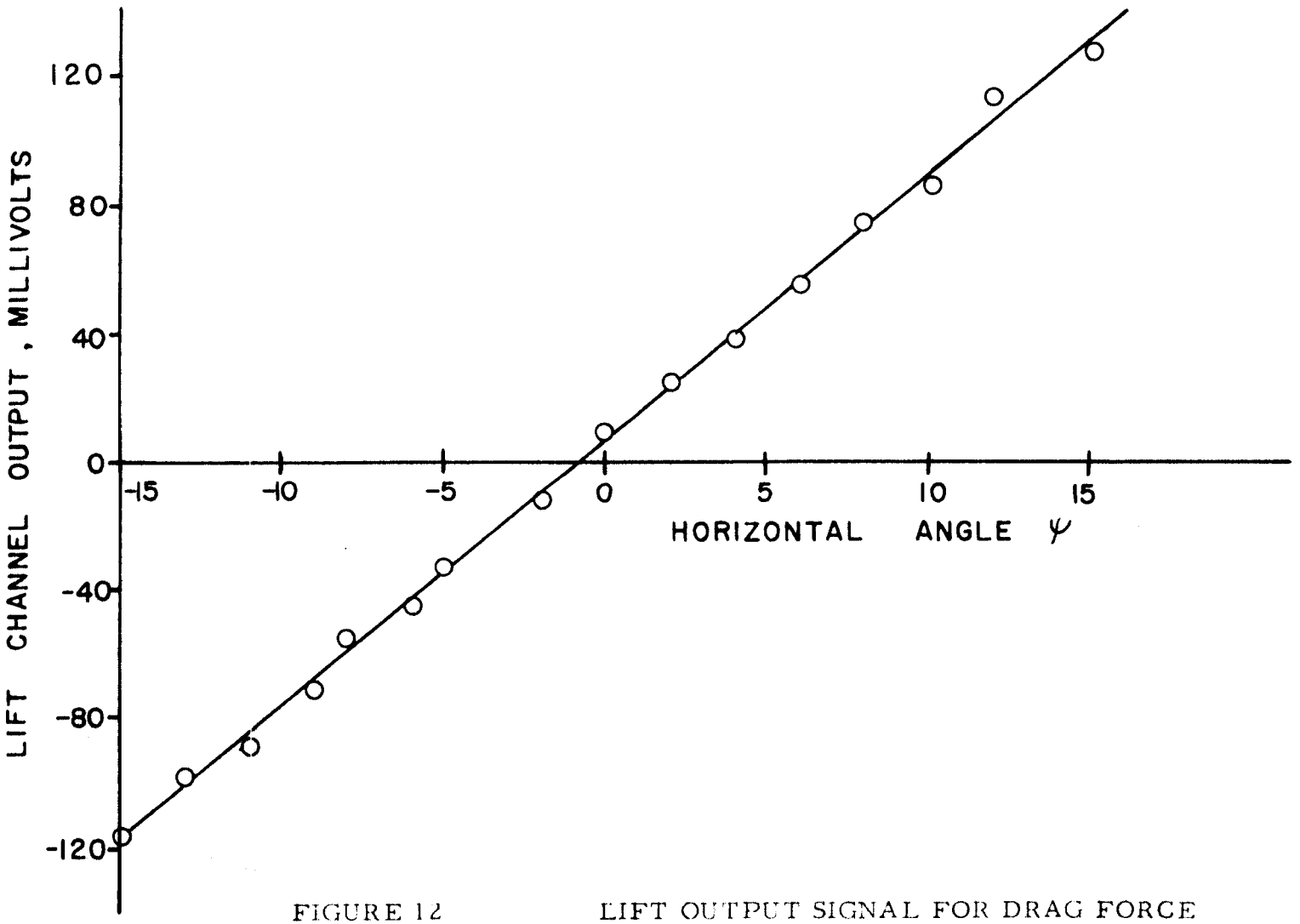

FIGURE 12 LIFT OUTPUT SIGNAL FOR DRAG FORCE AT $\psi = 0 \pm 15°$

The balance was then rotated through 90° to apply positive lift which was applied at 1° intervals for $\psi = 90° \pm 15°$ and drag was recorded and plotted as shown in Figure 13. A similiar procedure was used to load negative drag and negative lift and these results are shown in Figures 14 and 15 respectively.

The results of the four trials agreed within ±0.50° and the average of the four indicated the ± drag axes to be at an angle ψ of -.75° from the center line of the control motors. This deviation is probably due to misalignment of the motor torque arm holding the two permanent magnets with respect to the center line through the control motor coil pairs. The control system will position the motor torque arm at a null point producing zero output from the Z_1 and Z_2 sensors. If the centers of the transformer coils of these two sensors do not lie on a line parallel to the line joining the centers of coil pairs X_1 and X_2, an error will result. Figure 17 illustrates this effect in an exaggerated view. It is seen that due to misalignment, the transformer coil for sensor Z_1 is displaced a distance ΔZ from the line through the center of sensor Z_2 and parallel to the center line of coil pairs X_1 and X_2. Since the motor torque arm will follow the sensors, an error results producing ψ. Other possible causes are nonuniformity of the magnetic field produced by the control motor coils, and inexact alignment of the torque arm hardware, although the ΔZ offset of the transformer coils is probably the most predominant.

APPLICATION OF CALIBRATION LOADS
1--HIGH RANGE

Although the system was designed to have a 0.5# full load capacity, this capability had not been obtained at the time of calibration. It was found that for an applied lift or drag load of approximately 0.375#, the sting bottomed against the center walls of the lower bearing block. Thus, for all of the calibration runs, drag and lift calibration loads were limited to 0.360# or less. For this series of calibration runs, all three range switches on the readout box were set at the 0.5# position.

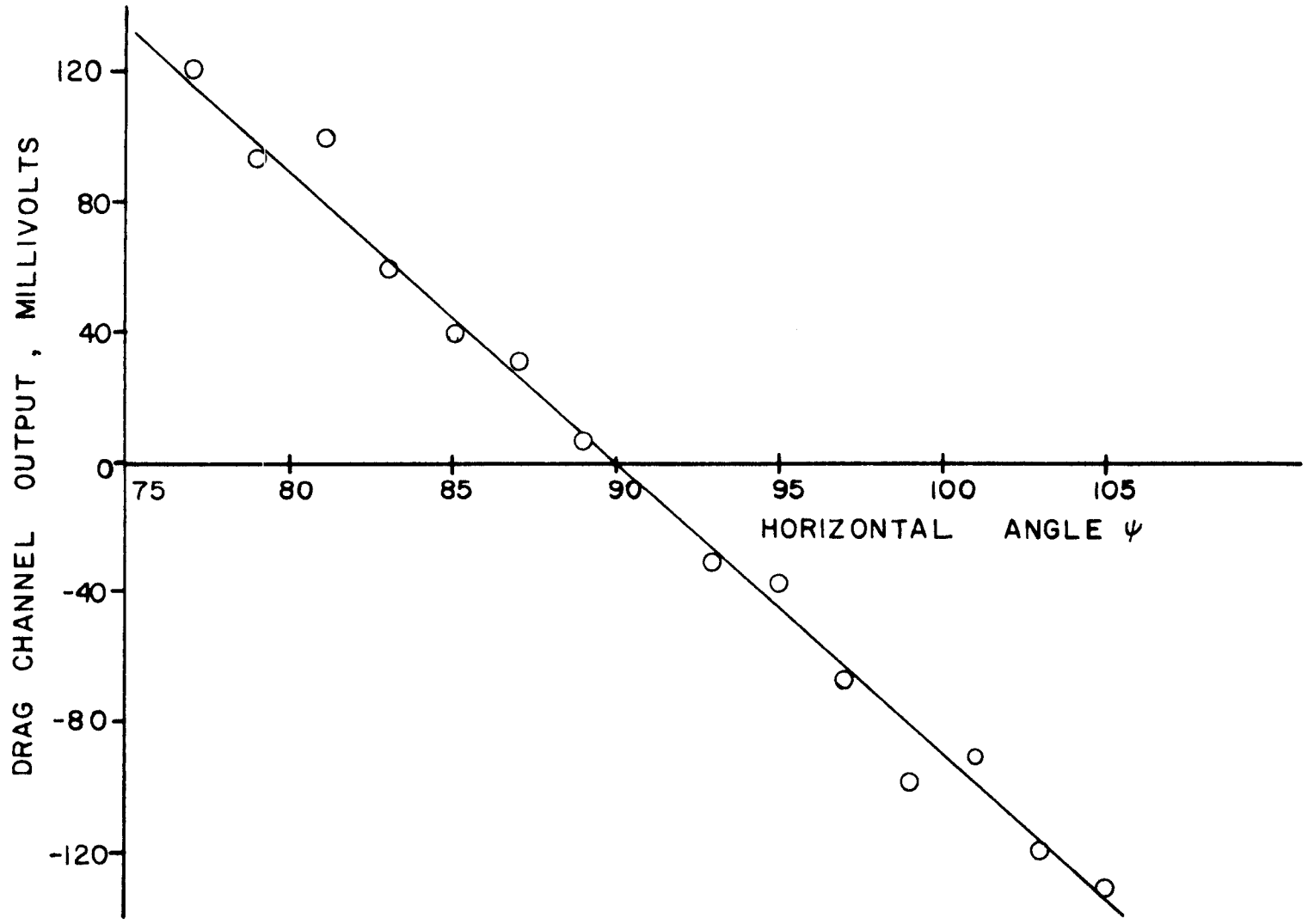

FIGURE 13 DRAG OUTPUT SIGNAL FOR LIFT FORCE AT $\psi = 90° \pm 15°$

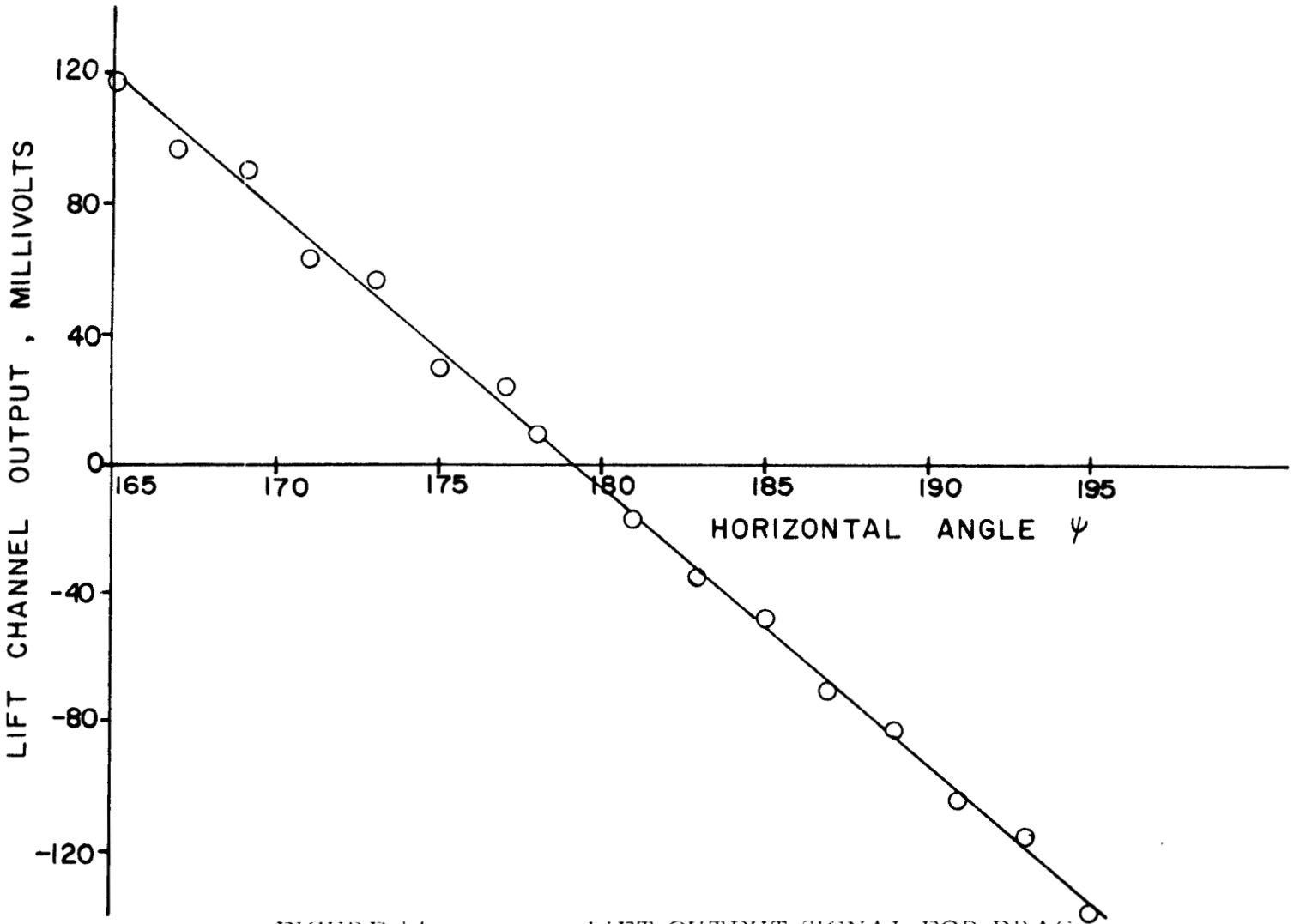

FIGURE 14 LIFT OUTPUT SIGNAL FOR DRAG FORCE AT $\psi = 180° \pm 15°$

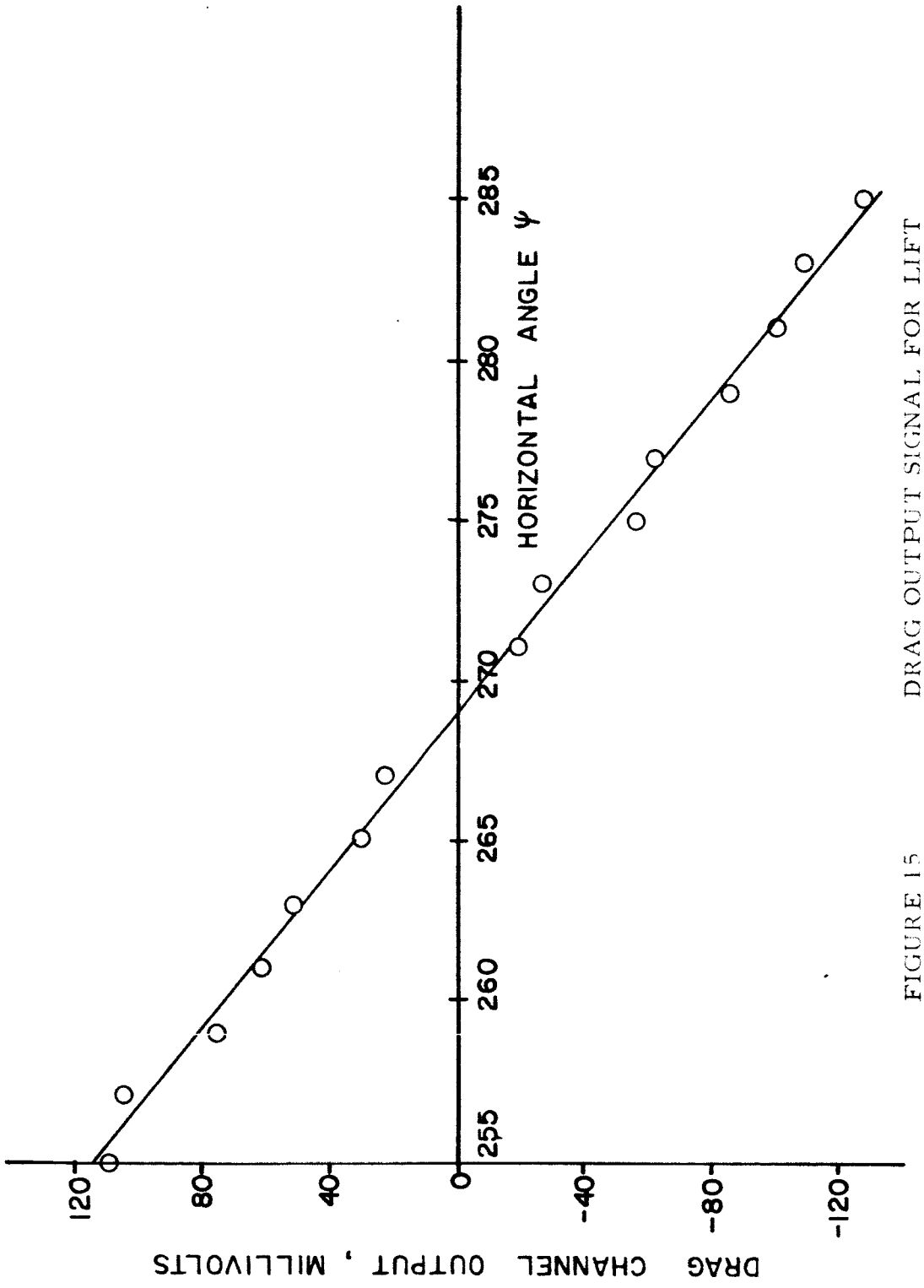

FIGURE 15 DRAG OUTPUT SIGNAL FOR LIFT FORCE AT $\psi = 270° \pm 15°$

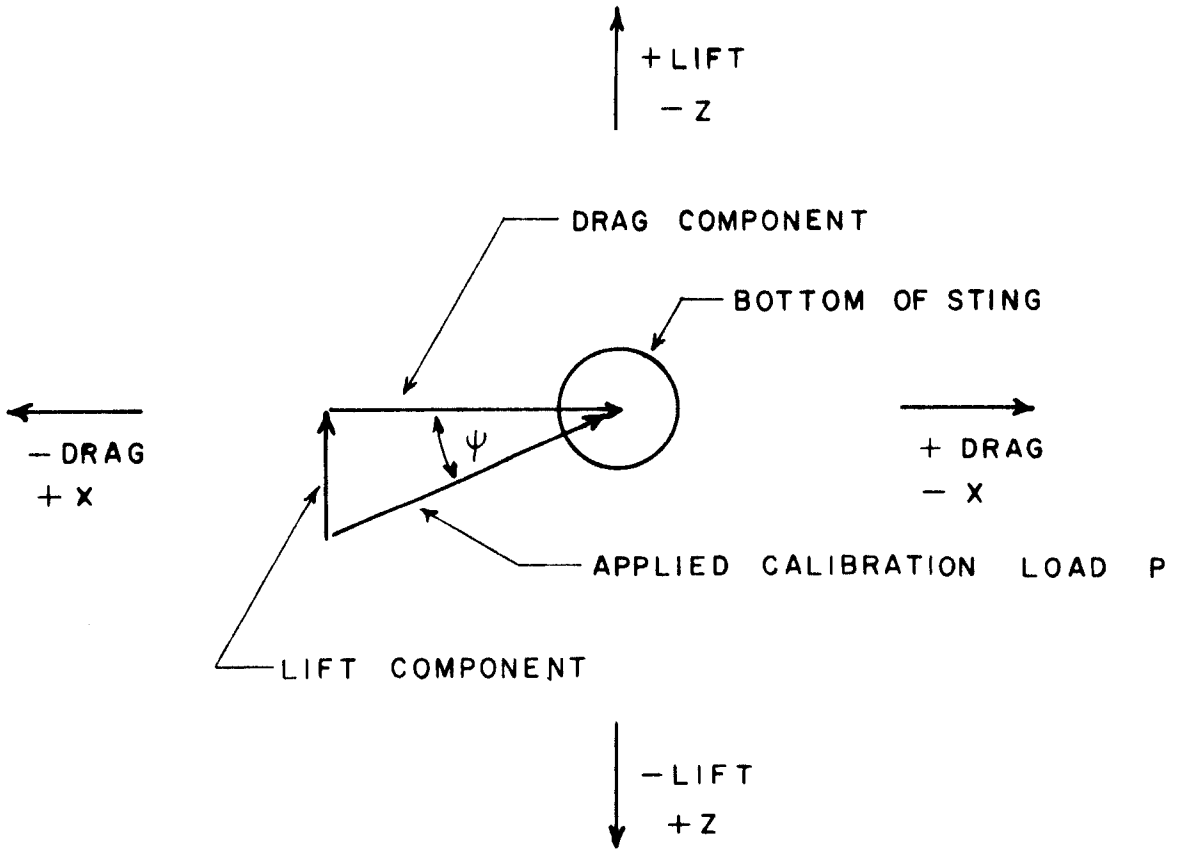

FIGURE 16 CALIBRATION LOAD COMPONENTS

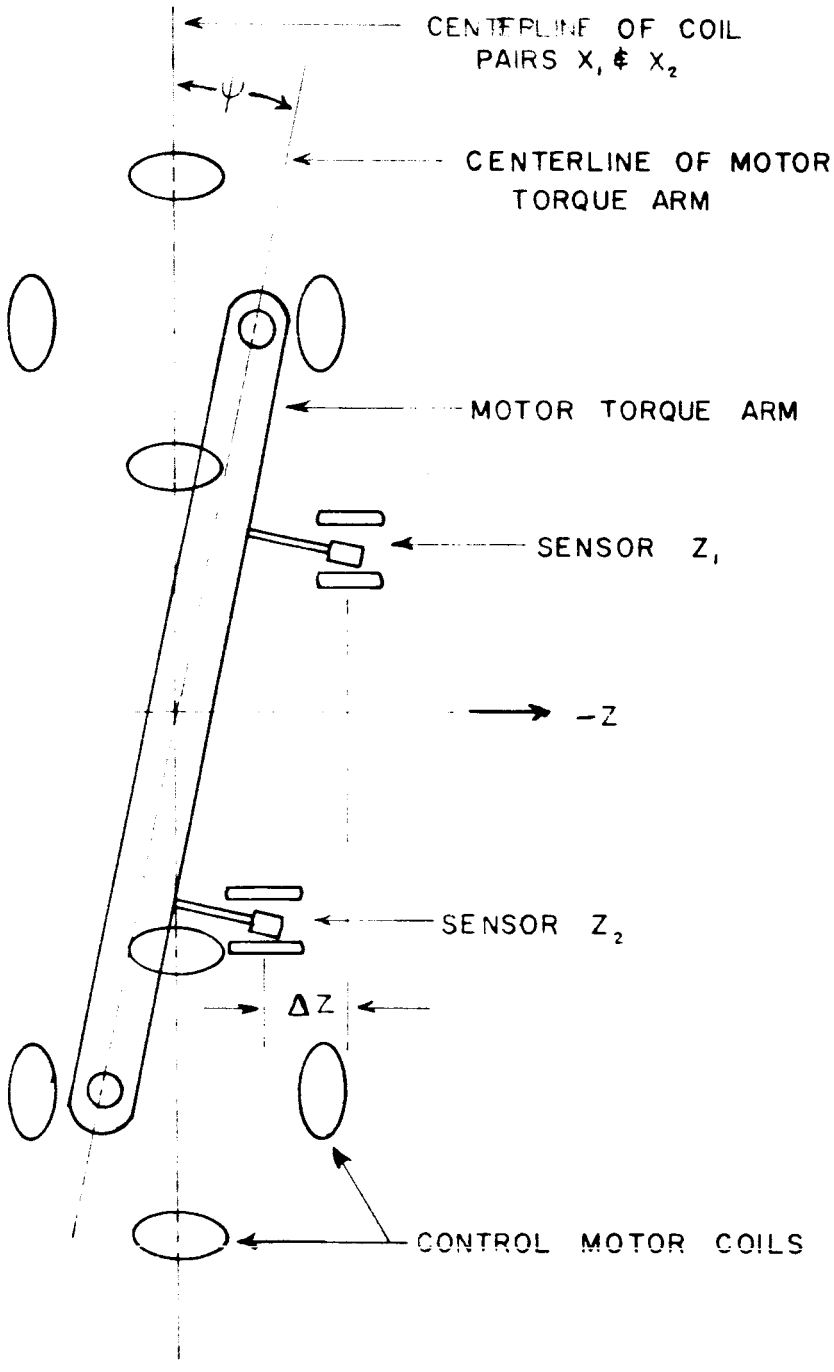

FIGURE 1 — SCHEMATIC ARRANGEMENT OF SERVOED SYSTEM AXIS

The readout signal of each of the three channels was measured using a DANA series 5600 digital volt meter.

DIRECT LOADS

Drag and Lift: The balance was turned to $\psi = -.75°$ and positive drag was applied in nine increments from zero to 0.3527#. The drag load was then removed in increments back to zero again to check for hysteresis. Three trials were run and for each load increment, the output signal of the drag, lift and pitch channels were read and recorded.

The balance was then turned back trhough 90° and positive lift was loaded for three trials in the same manner. Again, all three readout channels were read and recorded for each load increment. Finally, the balance was turned through 180° and negative lift was loaded for three trials with the same increments as before.

Application of Pitch: Pitching moment was applied by loading positive drag at $Z = \pm 15"$ on an aluminum moment arm attached to the bottom of the sting. One string force device was attached to each end of the moment arm as shown in Figure 18. Each pan was loaded with 50 gms and an initial reading of all three channels was taken. The weights were then transferred from pan A to pan B in ten increments to produce full positive pitch.

The weights were then transferred back to pan A from pan B until all weights were in pan A to provide full negative pitch. This process was repeated three times and readings of all three channels were recorded for each load increment.

COMBINED LOADS

Cross product coupling was determined by loading the system with two separate calibration forces. For example, to determine the D x L interaction coefficients, full positive lift was applied to the system and then drag was applied in 9 increments from zero to full load and then back to zero again. Then, full negative lift was applied and drag was

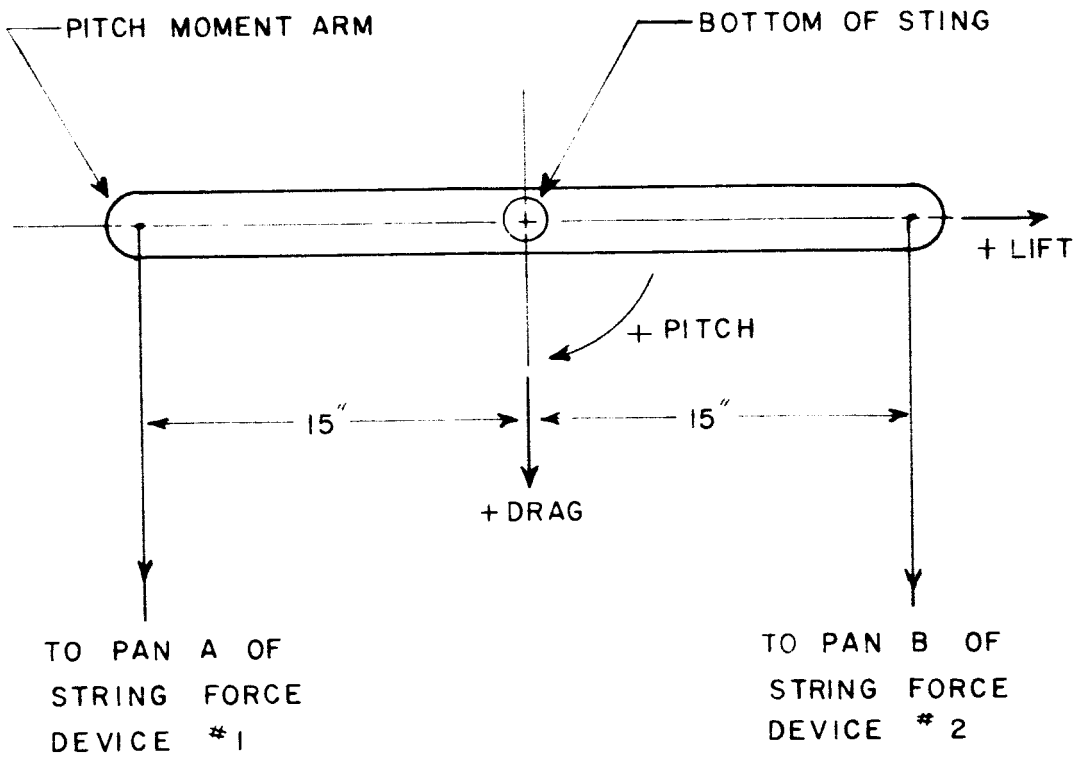

FIGURE 18 METHOD OF LOADING PITCH (TOP VIEW)

again loaded from zero to full load in 9 increments. The above process was repeated twice more to give three trials for each loading scheme. To determine the D x M interaction coefficient, full positive pitch was applied and then positive drag was loaded in increments from zero to full load. Then full negative pitch was applied and positive drag was again loaded in increments from zero to full load. A similiar procedure was used to determine the other coupling coefficients. Table I gives a summary of the loading combinations used to determine the cross product coupling coeffients. For each load increment of each load combination, the output signal of all three channels was read and recorded on the digital voltmeter.

2--LOW RANGE

All three of the range switches on the readout box were set at 0.05# for this series of calibration loads. The range switches on the readout box were wired to produce an output sensitivity on the 0.05# range of 10 times that of the 0.5# range. However, due to tolerances on the readout resistors, the attenuation factor was found to not be exactly 10 to 1 for the three channels.

DIRECT LOADS

The calibration loads were applied exactly in the same sequence as described for the high range except that each of the applied calibration loads was one-tenth that of the corresponding load used for high range. For this range, however, the sting force devices were used to apply lift and drag instead of the analytical balance. The reason for this was that the balance was found to have static friction, producing an error of approximately 1.0% of the applied calibration load for this low range.

COMBINED LOADS

It was found that the accurate determination of cross coupling effects

TABLE I

LOADING COMBINATIONS

Run No.	Primary Load (Loaded in increments from zero to full load)	Secondary (Constant load)
1	+ Drag	+ Lift
2	+ Drag	- Lift
3	+ Drag	+ Pitch
4	+ Drag	- Pitch
5	+ Lift	+ Drag
6	- Lift	+ Drag
7	+ Lift	+ Pitch
8	+ Lift	- Pitch
9	- Lift	+ Pitch
10	- Lift	- Pitch
11	+ Pitch	+ Drag
12	- Pitch	+ Drag
13	+ Pitch	+ Lift
14	+ Pitch	- Lift
15	- Pitch	+ Lift
16	- Pitch	- Lift

for this range was impossible due to a high percentage of background noise. The random background noise due to electronic noise and room background vibrations was found to be of a fairly constant magnitude. On the high range, this background noise caused fluctuations in the three readout channel outputs of approximately ±0.1% on the lower loads for that range. However, on the low range (0.05#), the noise fluctuations amounted to ±1% or more of the readout signal. Since the cross coupling was less than 1% as determined from the high range calibration data, it was masked by the system noise to the extent that it was impossible to determine the exact magnitude of the cross coupling. All that could be said was that the cross coupling effects were less than ±1%. Thus, only a sensitivity constant was determined for each channel on the lower range setting. A more complete analysis of this noise problem along with a discussion of possible methods to eliminate it is included in the section of Chapter V dealing with "Scatter of Output Data" and in Chapter VII in the section on "Background Vibrations."

REDUCTION OF DATA

Three trials were made for each loading combination except for the loading of lift and drag on the 0.05# range. In these two cases, where random output variations were relatively large, five trials were made to insure a better average value. In cases where the output signal was fluctuating between two boundaries, a reading half way between these boundaries was taken. The outer boundaries were also recorded to give a measure of the scatter of the readings.

The three, (or five), output readings for each channel and each load combination were averaged and the average initial reading subtracted to give a net average reading for each load increment. The resultant average output was plotted vs-the applied calibration load using an expanded scale technique as described below.

PLOTTING METHOD

In the plotting of the readout voltage-vs-calibration load, it was desired to use as large a scale as possible to give the necessary precision to the plots. A linear plot with a scale range of 0-1000mv with enough precision to read 0.1mv would require a tremendously large plot. To provide the same precision on a smaller plot, the readout voltage was reduced by an amount proportional to the load. The following example, given in Table II, illustrates the use of this technique.

LOAD (#)	OUTPUT (mv)	ADJUSTMENT (100mv/1b)	NET (mv)
0	0		
1	101.1	100	1.1
2	202.2	200	2.2
3	303.4	300	3.4

TABLE II
EXAMPLE OF EXPANDED SCALE ADJUSTMENT

The net output is plotted vs the applied load and provides a much more sensitive check on the linearity and random variations of the output signal than a plot of the full output-vs-load. The actual plots made to determine the sensitivity constants and interaction coefficients were made on 25 x 38 cm graph paper. The plots contained in this thesis are scaled down copies of the orginals and as such do not reflect the precision obtainable with the larger plots.

CHECK ON CALIBRATION DATA WITH DIGITAL COMPUTER

The University's Burroughs B5500 digital computer was used to

check the calibration data. The computer was used to fit first, second, and third order polynomials to the calibration data using a least squares error technique to obtain the best possible curve fit. Trials were made first with the calibration loads to be the adjusted variable for minimum error and then with the output signal to be adjusted for minimum error. The computer determined the coefficients of the zero, first, second, and third order terms of the polynomial expression.

The computer checks indicated two things about the data. First, it was found that the slopes of the output curves as determined by the expanded scale plotting technique were within ±0.1% of those determined by the least squares computer fit. This indicated that the expanded scale plotting technique gave a good method of fitting a first order curve to a set of data points.

Secondly, it was found that the second order terms of the calibration curves were very small. All of the data sets indicated second order terms to be less than ±0.2%, and in most cases, less than the point to point variation of the output signal. Thus, it was only possible to determine the first order calibration coefficients for the system equations.

DETERMINATION OF CALIBRATION EQUATION COEFFICIENTS

The calibration equation coefficients for each channel were determined from the plots of applied calibration load (or loads)-vs-channel output. The determination of these coefficients for the drag channel on 0.5# range is carried out below and illustrates the general procedure used for the other channels as well.

The actual output signal is the sum of the adjusted output and the adjustment signal for that particular loading. The adjusted output is read off of the calibration plot for a particular load. The adjustment signal is the product of the adjustment constant and the particular load.

For example, the adjusted output for a pure positive drag load of 0.3600# is found from curve A of Figure 19. This value is 20.5mv. The adjustment signal is (0.3600#) x (2350mv/lb) = 846 mv. Thus, the total drag channel output for a pure drag load of 0.3600# is 20.5mv +

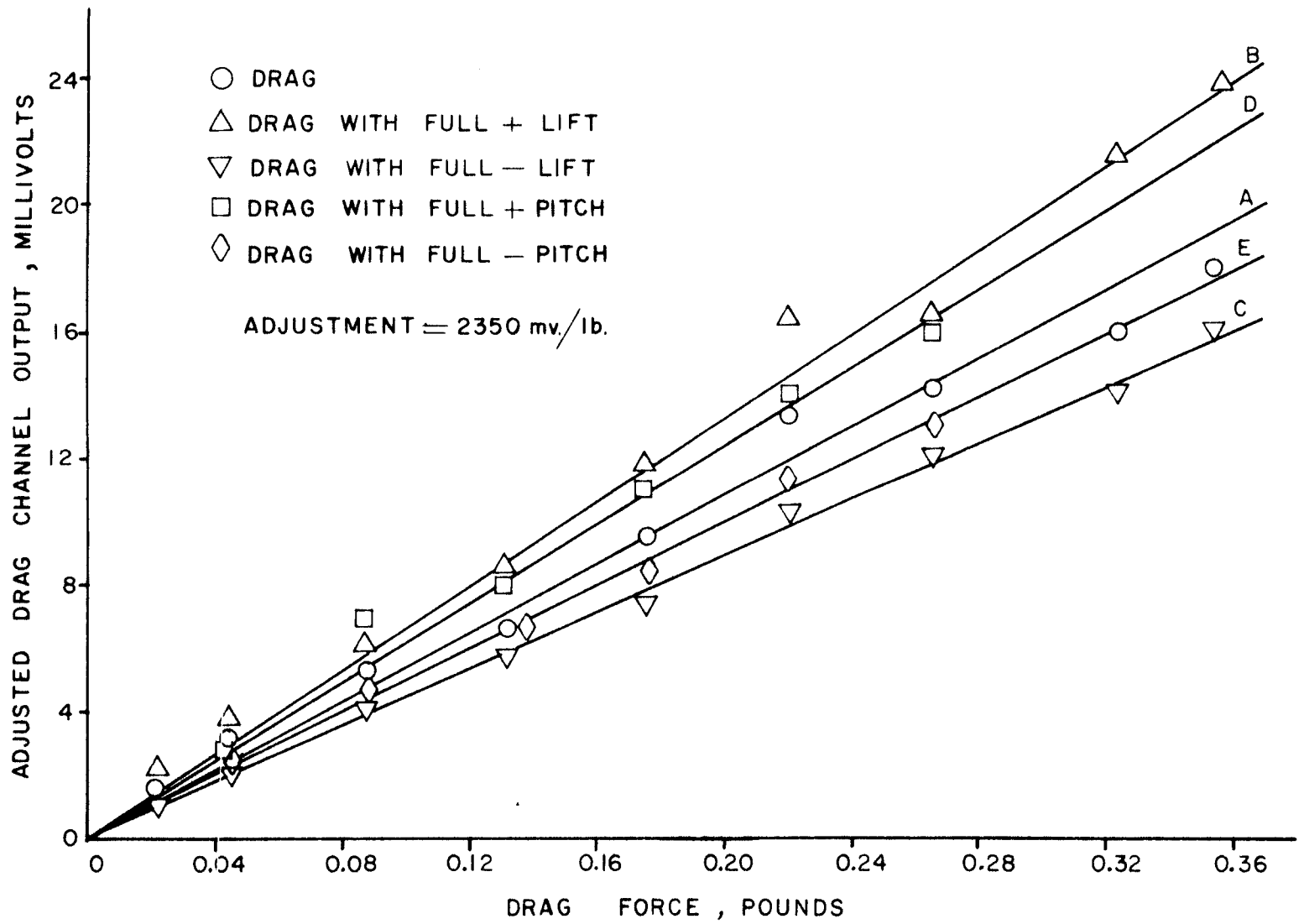

FIGURE 19 DRAG CHANNEL OUTPUT VS + DRAG FORCE

846 mv = 866.5 mv. For comparisons of output signals of different loading combinations such as A, B, C, etc., at any one load, it is only necessary to compare the adjusted output signal rather than the total output.

Determination of Sensitivity Constant. The sensitivity constant for a particular channel relates the total full scale output signal to the pure load applied. The sensitivity constant for + drag (k_{DD}) is found as follows:

$$k_{DD} = \frac{1}{K_{DD}} = \frac{\text{Drag Load (pounds)}}{\text{Drag Channel Output due to Pure Drag } (\theta_{DD})} = \frac{0.360\#}{866.5\text{mv}}$$

$$\therefore \quad k_{DD} = 4.155 \times 10^{-4} \text{ pounds/mv}$$

Determination of k_{DL}. Curve A of Figure 20 is a plot of the drag channel output for positive lift applied to the system. Curve A of Figure 21 is a similiar plot of drag channel output for applied negative lift. It is seen that a positive lift load produces a positive drag channel output proportional to that load and negative lift produces a similiar negative drag channel output. Thus, this interaction is a positive one[8]. The average magnitude of this effect for full positive and negative lift is θ_{DL}.

Where $\theta_{DL} = \frac{+1.7 + 1.8}{2} = 1.75$ mv for ± lift = 0.3600#

$$k_{DL} = \frac{\theta_{DL}}{L} \times k_{DD} = \frac{1.75}{.3600\#} \times 4.155 \times 10^{-4} = +2.0197 \times 10^{-3}$$

---

[8]Guarino, op. cit., p. 7.

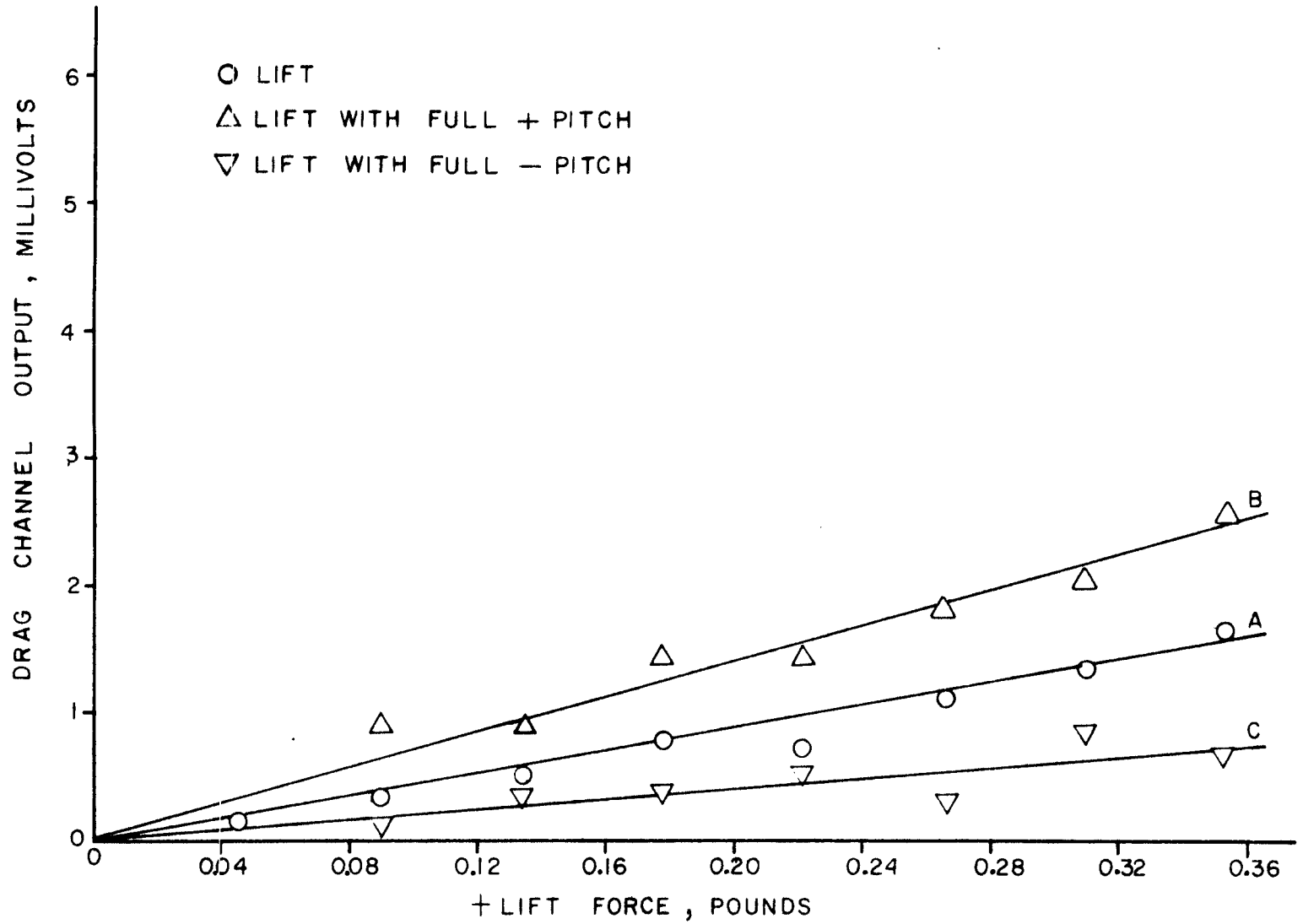

FIGURE 20 DRAG CHANNEL OUTPUT VS · LIFT FORCE

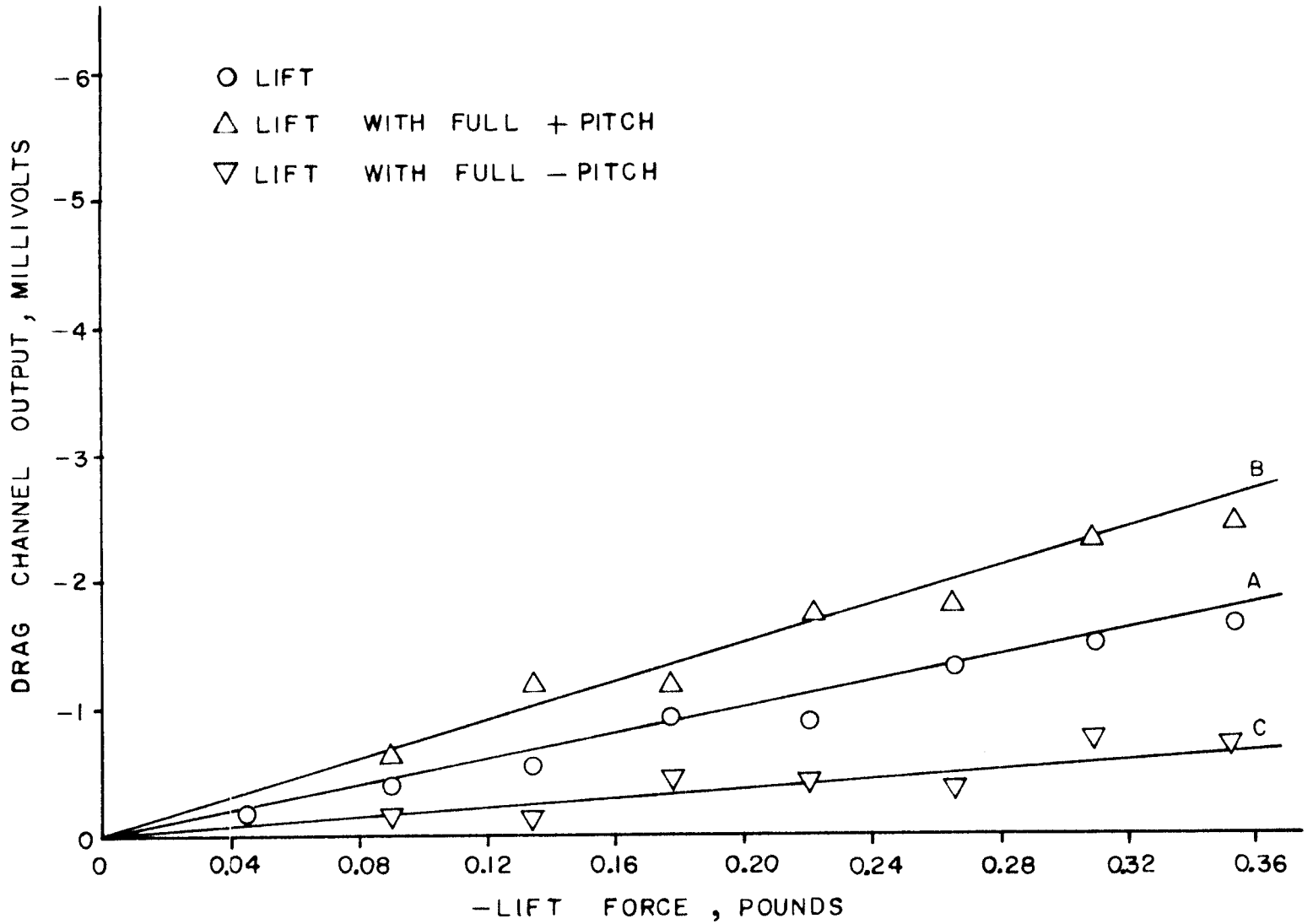

FIGURE 21 DRAG CHANNEL OUTPUT VS - LIFT FORCE

Determination of k_{DM}. Figures 22 and 23 are plots of the drag channel output for positive and negative pitching moments respectively. The interaction is a positive one since positive pitch produces a positive drag channel output. The average of the output signals at full positive and negative pitch moments of 1.8 inch-pounds is θ_{DM}.

$$\theta_{DM} = \frac{5 + 7.6}{2} = 6.3 \text{ mv}$$

$$k_{DM} = \frac{\theta_{DM}}{M} \times k_{DD} = \frac{6.3 \text{ mv}}{1.8 \text{ inch-pound}} \times 4.155 \times 10^{-4} =$$

$$+ 1.4542 \times 10^{-3} \frac{\text{pound}}{\text{inch-pound}}$$

Determination of k_{DD^2}, k_{DL^2}, and k_{DM^2}. As discussed in the section on computer polynomial curve fitting, the second order terms were found to be very small. The magnitude of these terms was less than the random variations of the data points and thus unreliable. Thus, it was assumed that these terms were small enough to be considered zero and the constants associated with them (k_{DD^2}, k_{DL^2}, and k_{DM^2}) were not determined.

Determination of k_{DDL}. Curves B and C of Figure 19 are plots of the drag channel output for applied drag load with full positive and negative lift respectively. It is seen that full positive lift causes the drag channel output to be larger for a given drag load than it is without it. Similarly, a negative lift load reduces the drag output. The magnitude of this shift of output curve from A to B or C is proportional to the product of drag load x lift load. The interaction is positive since a positive lift x a positive drag produces a positive shift in the drag channel output. The magnitude of this shift from A to B is 25.2 - 20.5 = + 4.7 mv for a positive 0.3600# lift load. The shift from B to C is + 16.8 - 20.5 = - 3.7 mv for a negative 0.3600# lift load. The average of the two is θ_{DDL}, where:

$$\theta_{DDL} = \frac{4.7 + 3.7}{2} = + 4.2 \text{ mv}$$

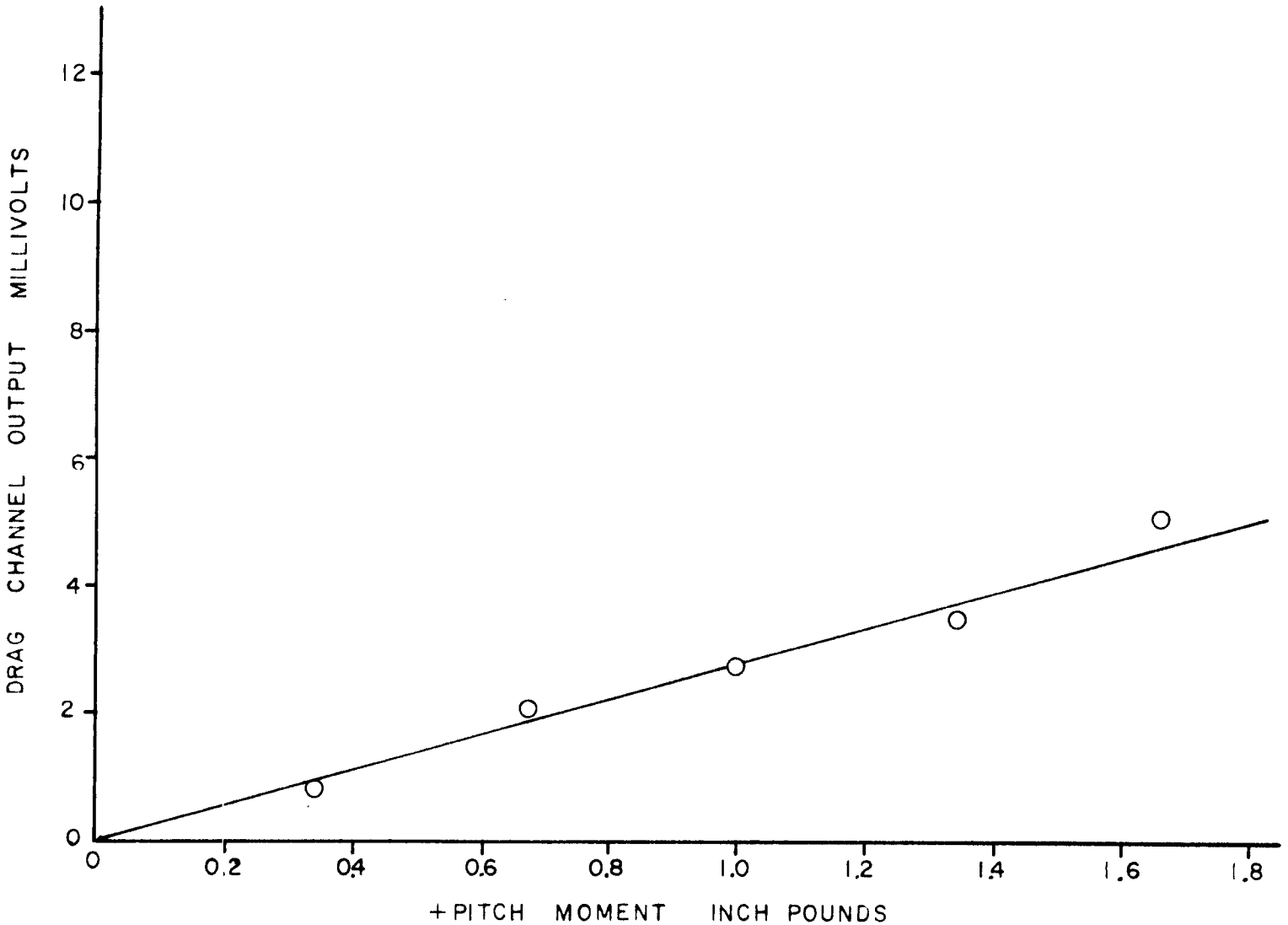

FIGURE 22 DRAG CHANNEL OUTPUT VS + PITCH FORCE

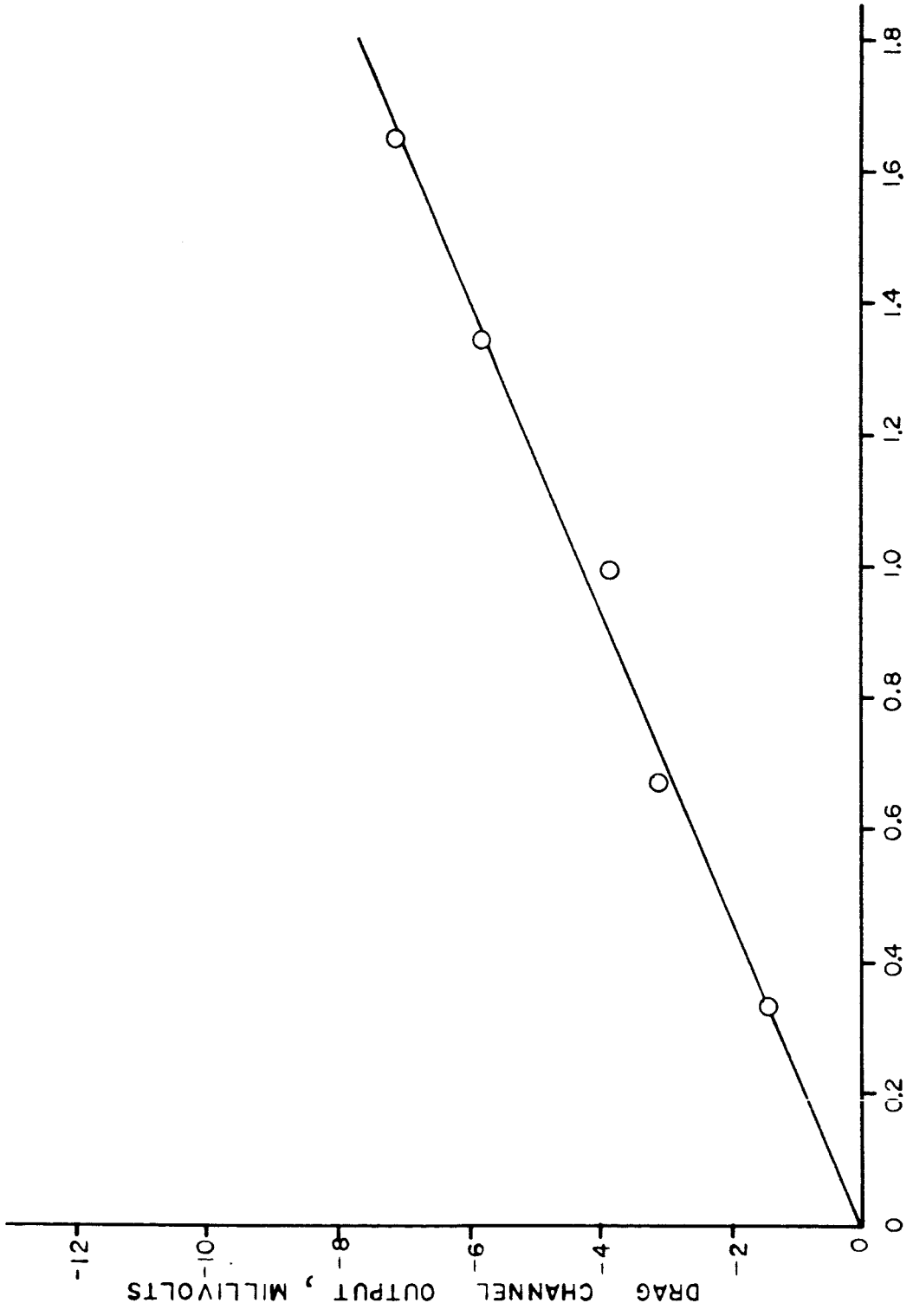

FIGURE 2[illegible] DRAG CHANNEL OUTPUT VS - PITCH FORCE

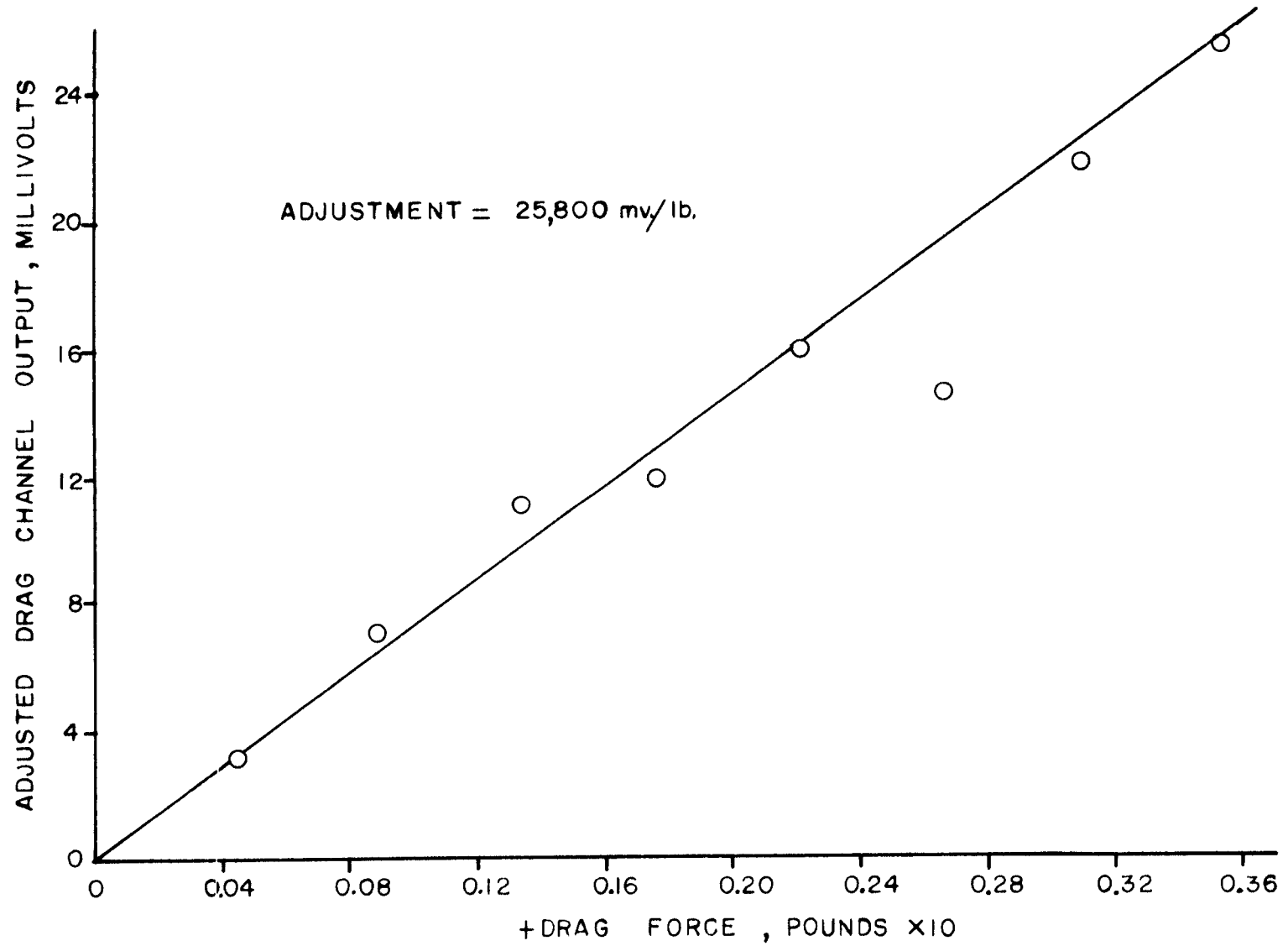

FIGURE 24 DRAG CHANNEL OUTPUT VS · DRAG FORCE, LOW RANGE

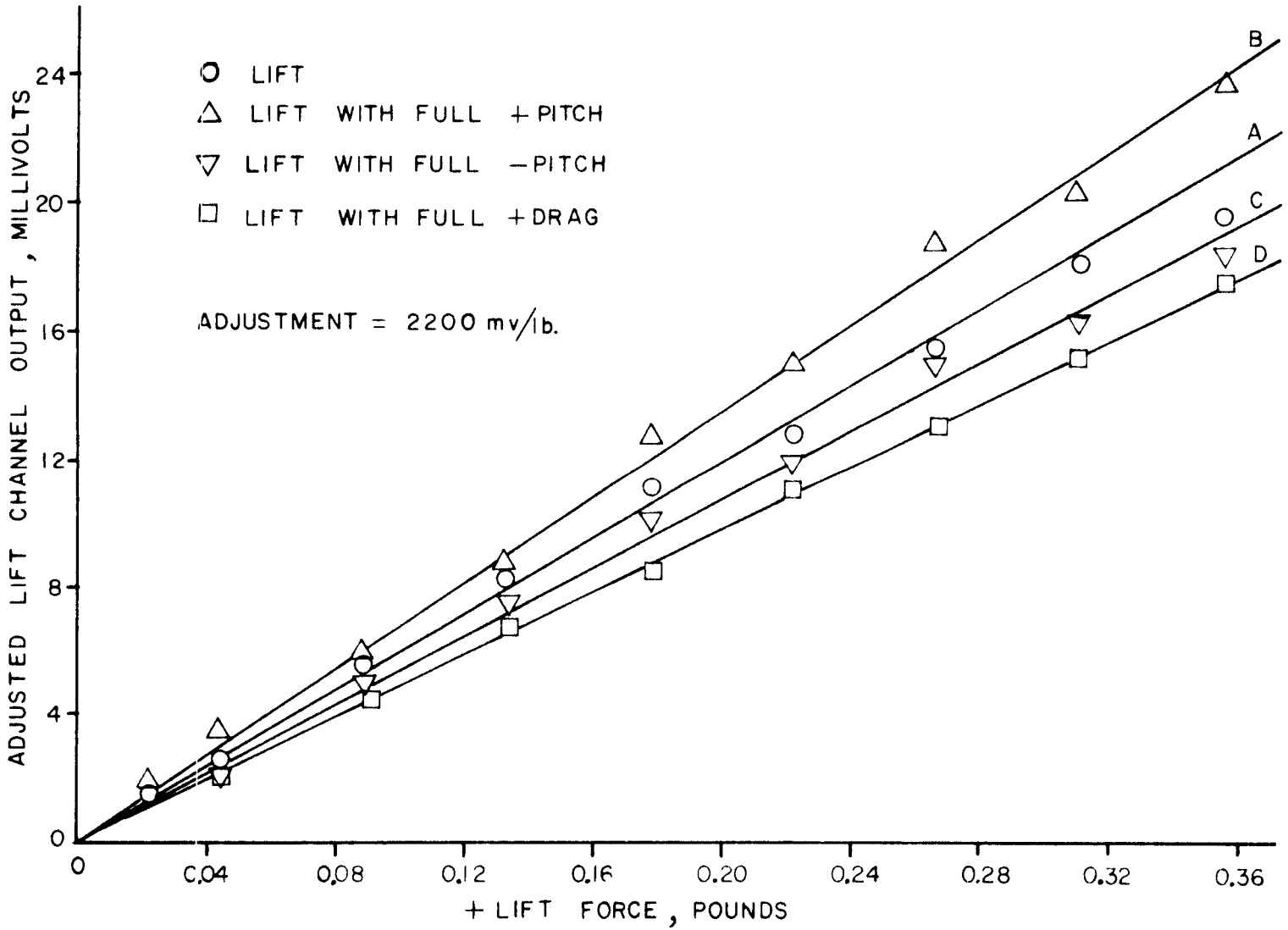

FIGURE 25 LIFT CHANNEL OUTPUT VS + LIFT FORCE

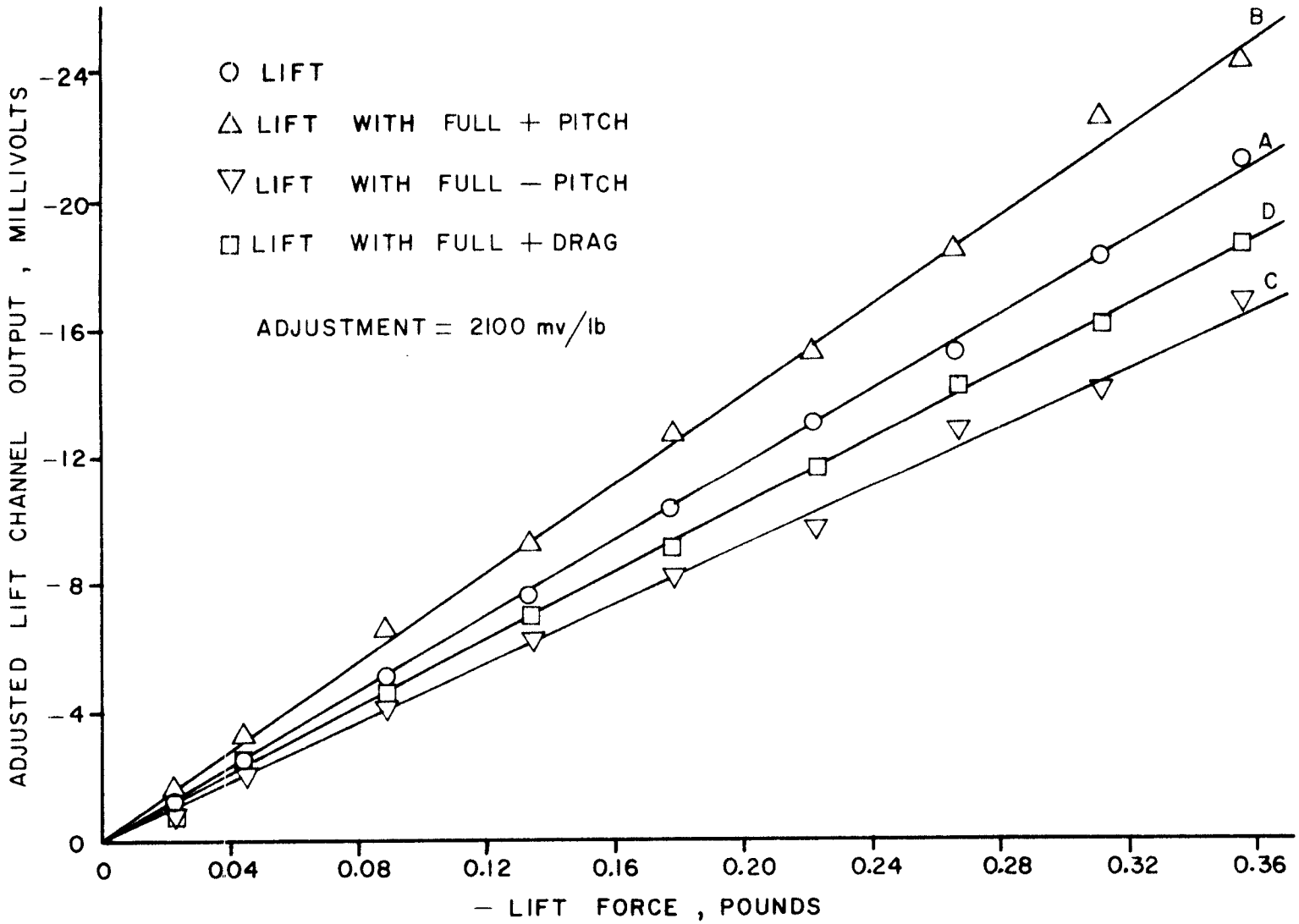

FIGURE 26 LIFT CHANNEL OUTPUT VS - LIFT FORCE

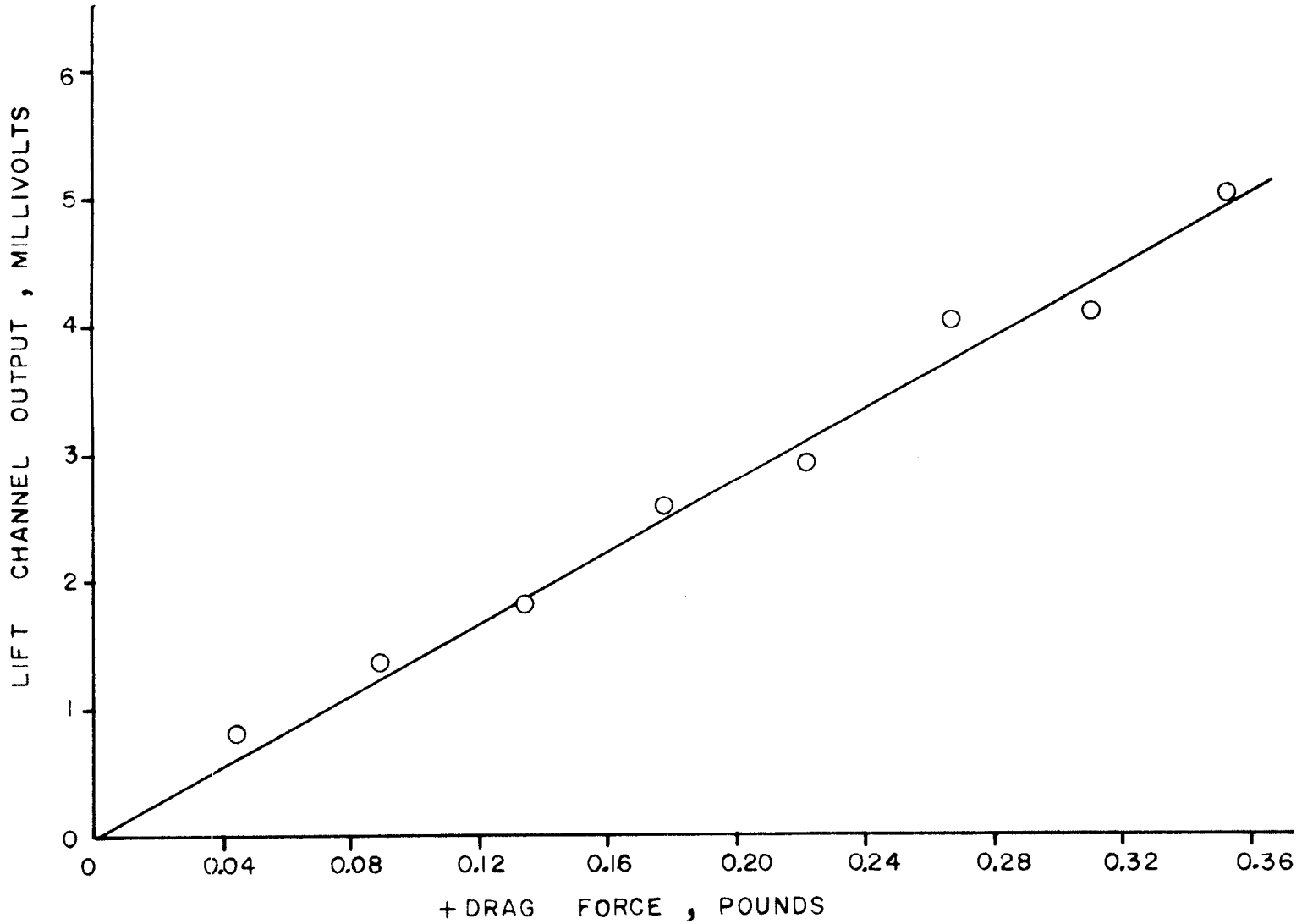

FIGURE 27 LIFT CHANNEL OUTPUT VS + DRAG FORCE

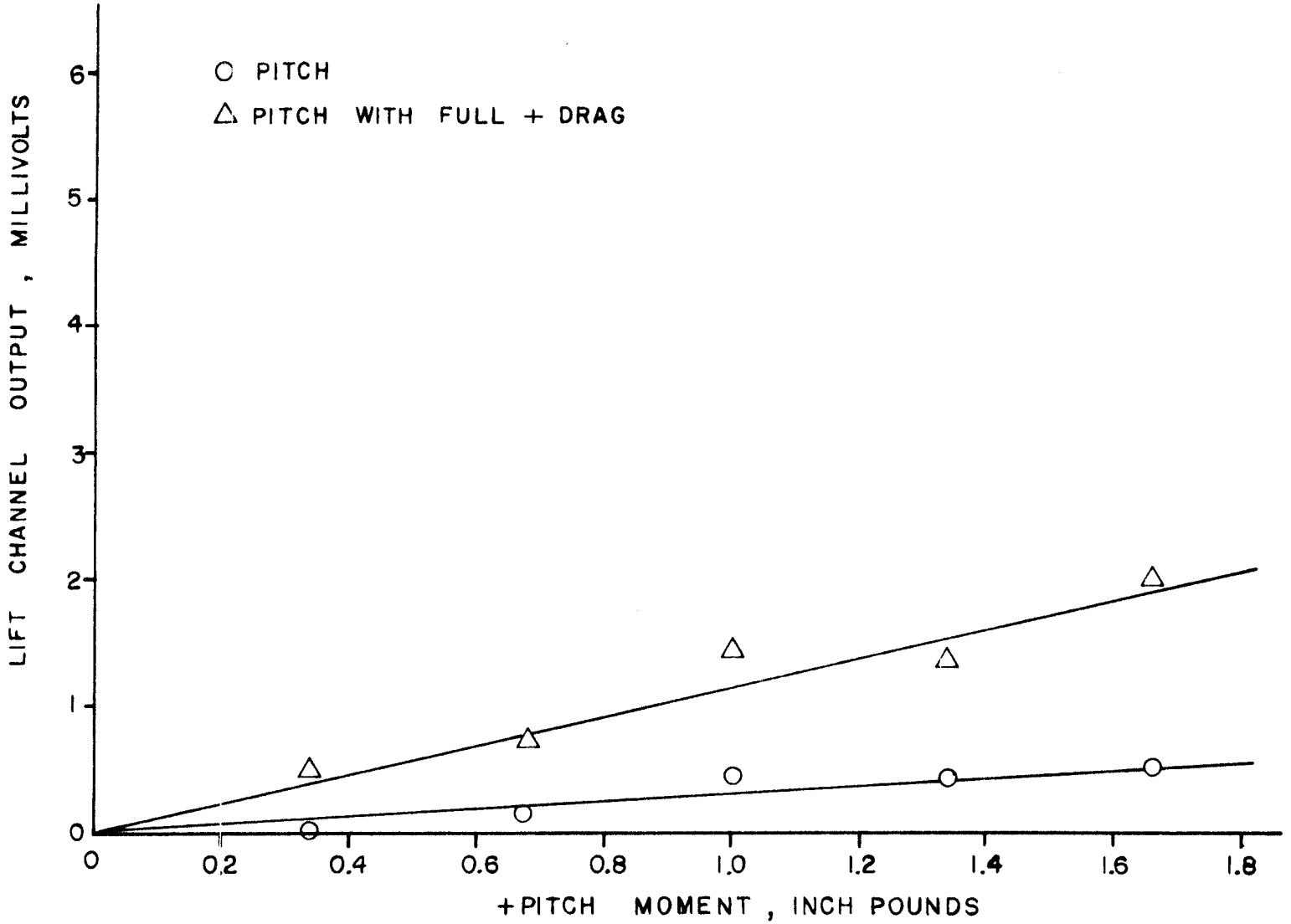

FIGURE 28 LIFT CHANNEL OUTPUT VS + PITCH MOMENT

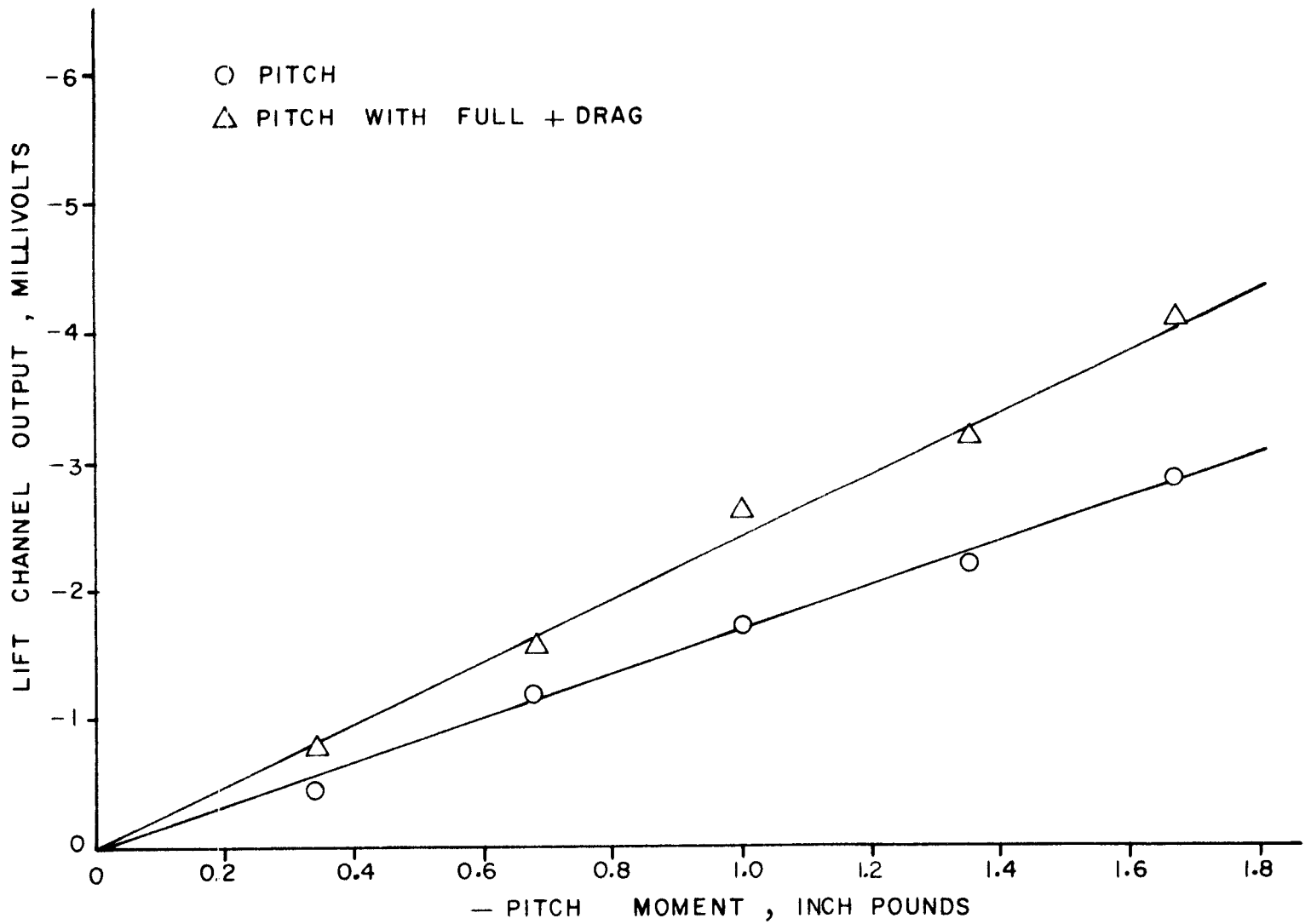

FIGURE 29 LIFT CHANNEL OUTPUT VS - PITCH MOMENT

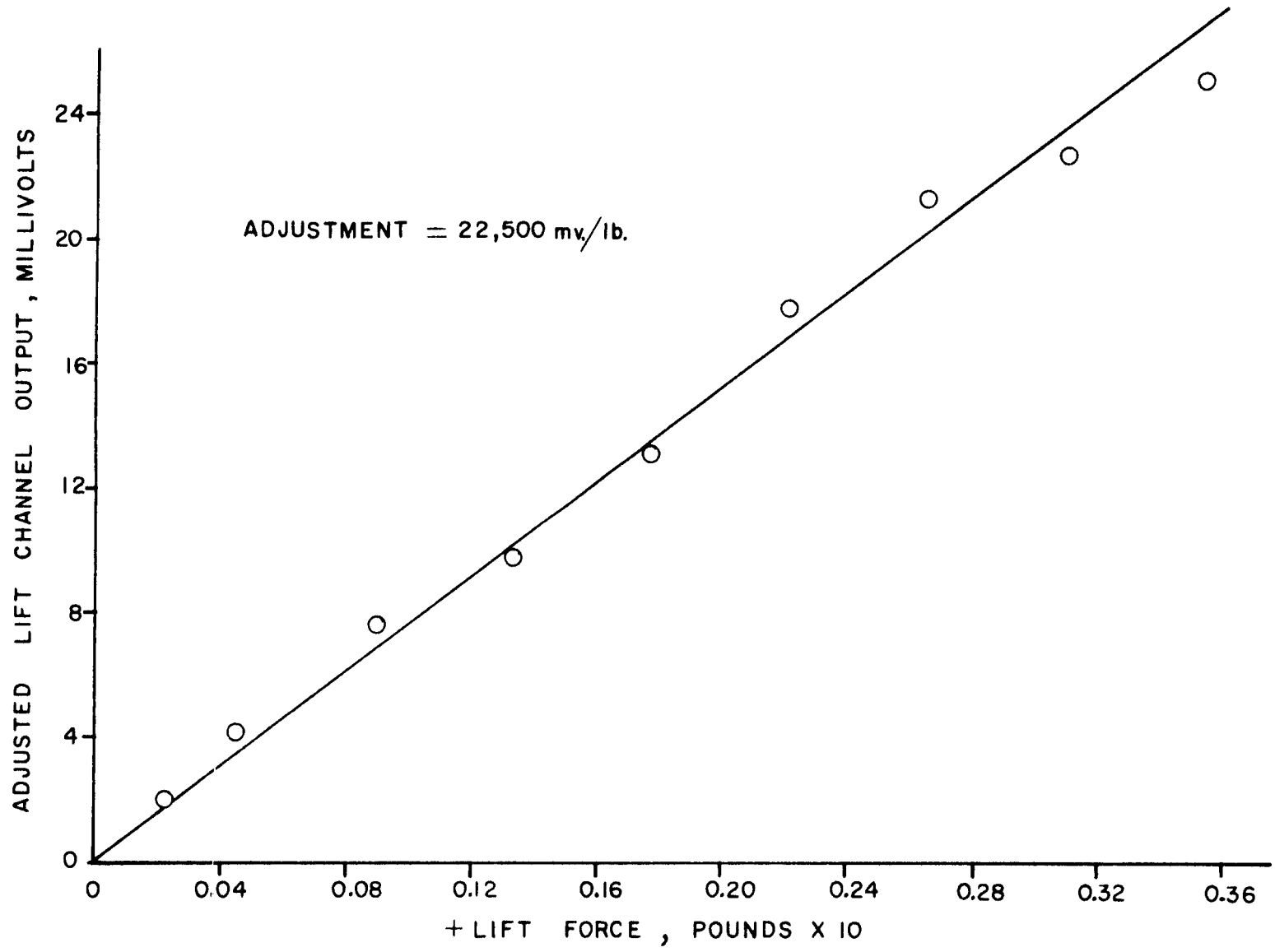

FIGURE 30 LIFT CHANNEL OUTPUT VS + LIFT FORCE, LOW RANGE

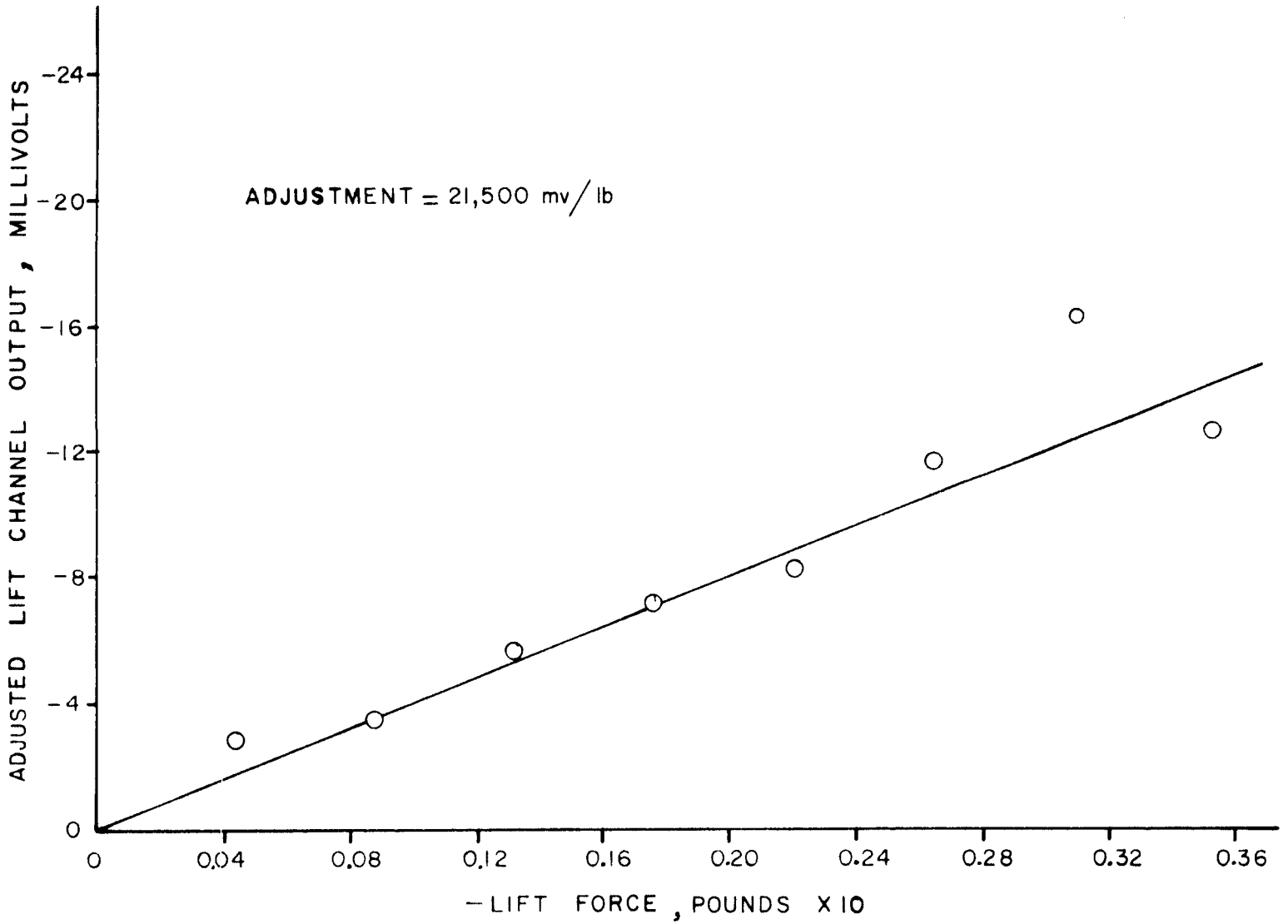

FIGURE 31 LIFT CHANNEL OUTPUT VS - LIFT FORCE, LOW RANGE

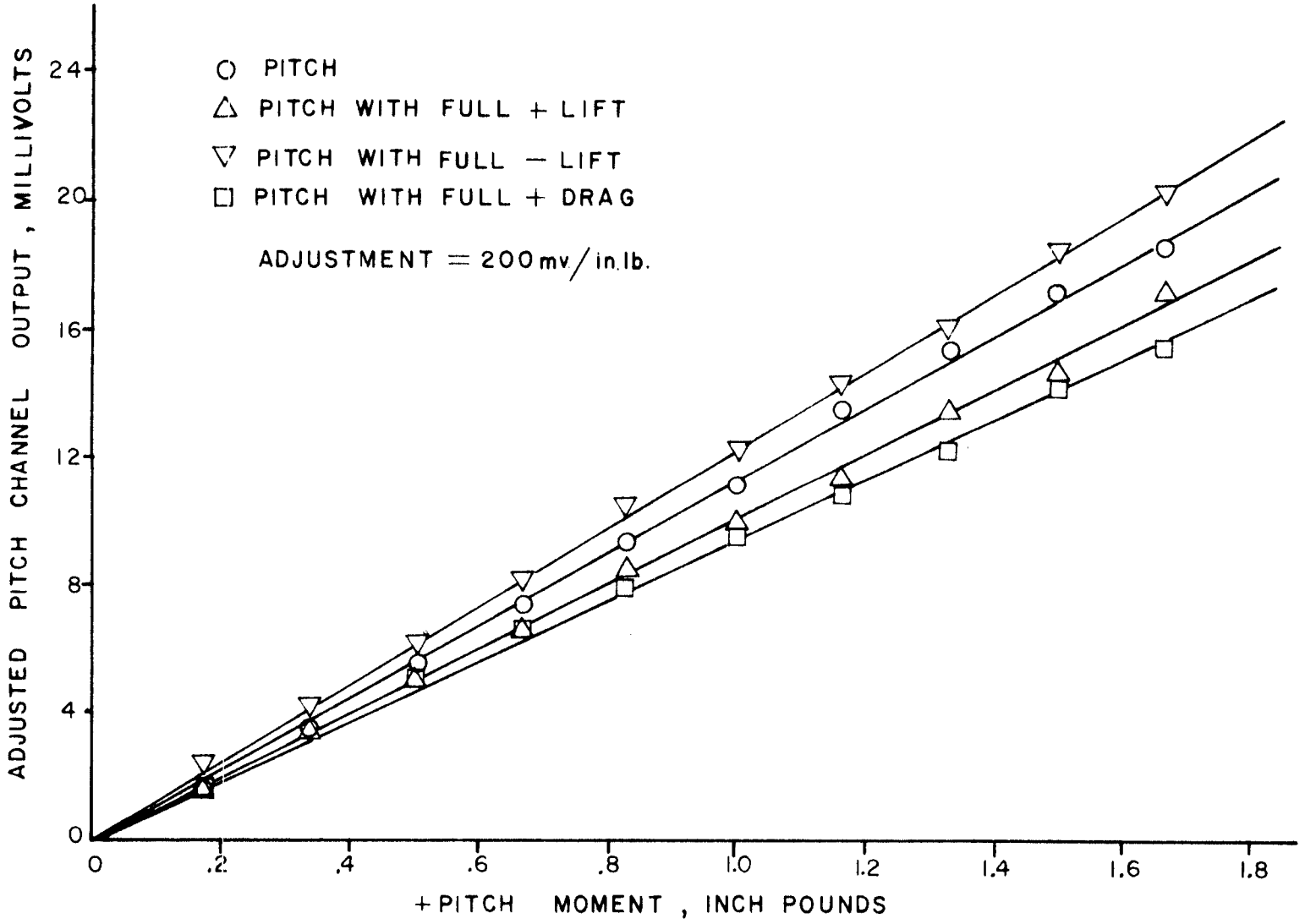

FIGURE 52 PITCH CHANNEL OUTPUT VS + PITCH MOMENT

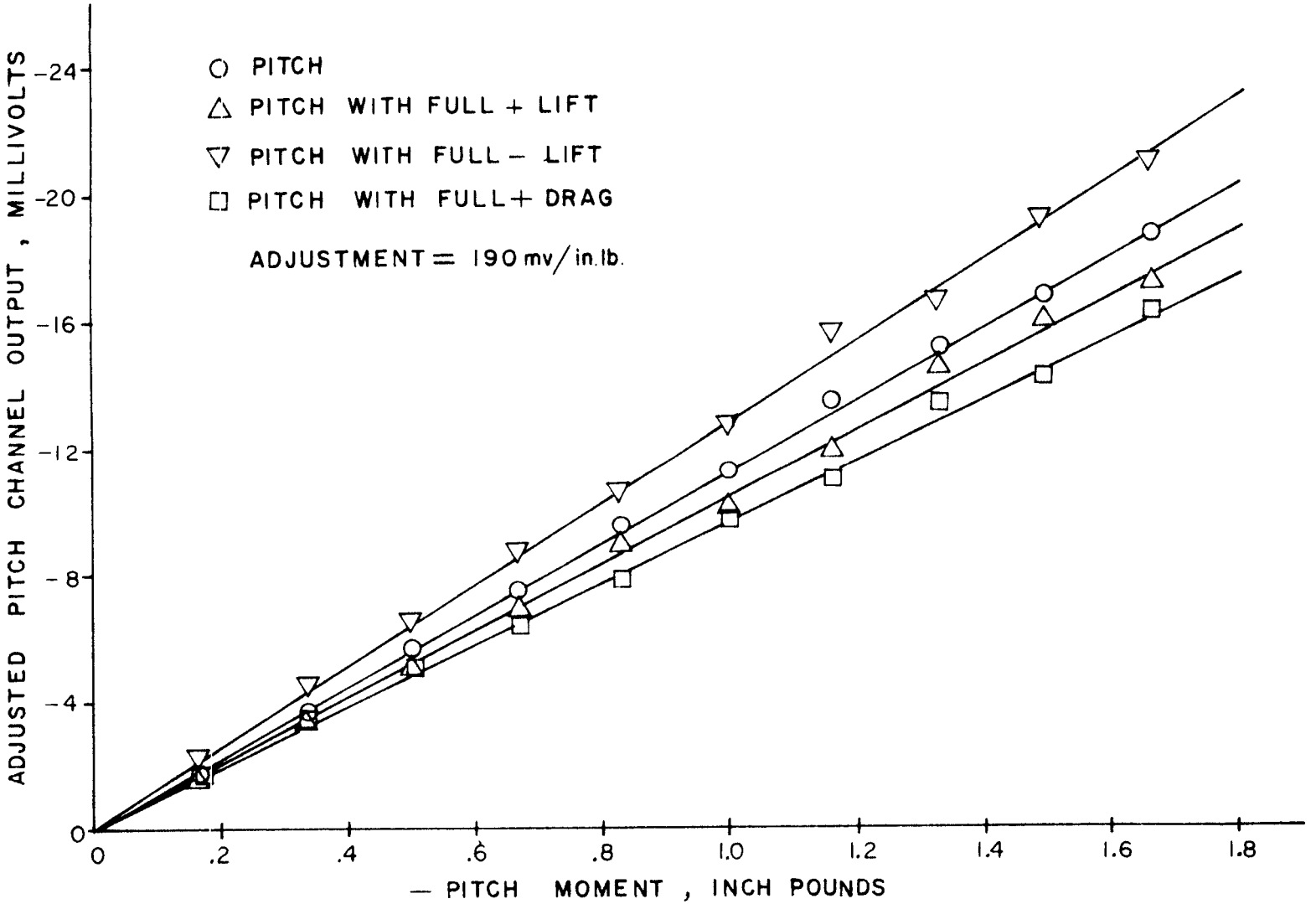

FIGURE 55 PITCH CHANNEL OUTPUT VS - PITCH MOMENT

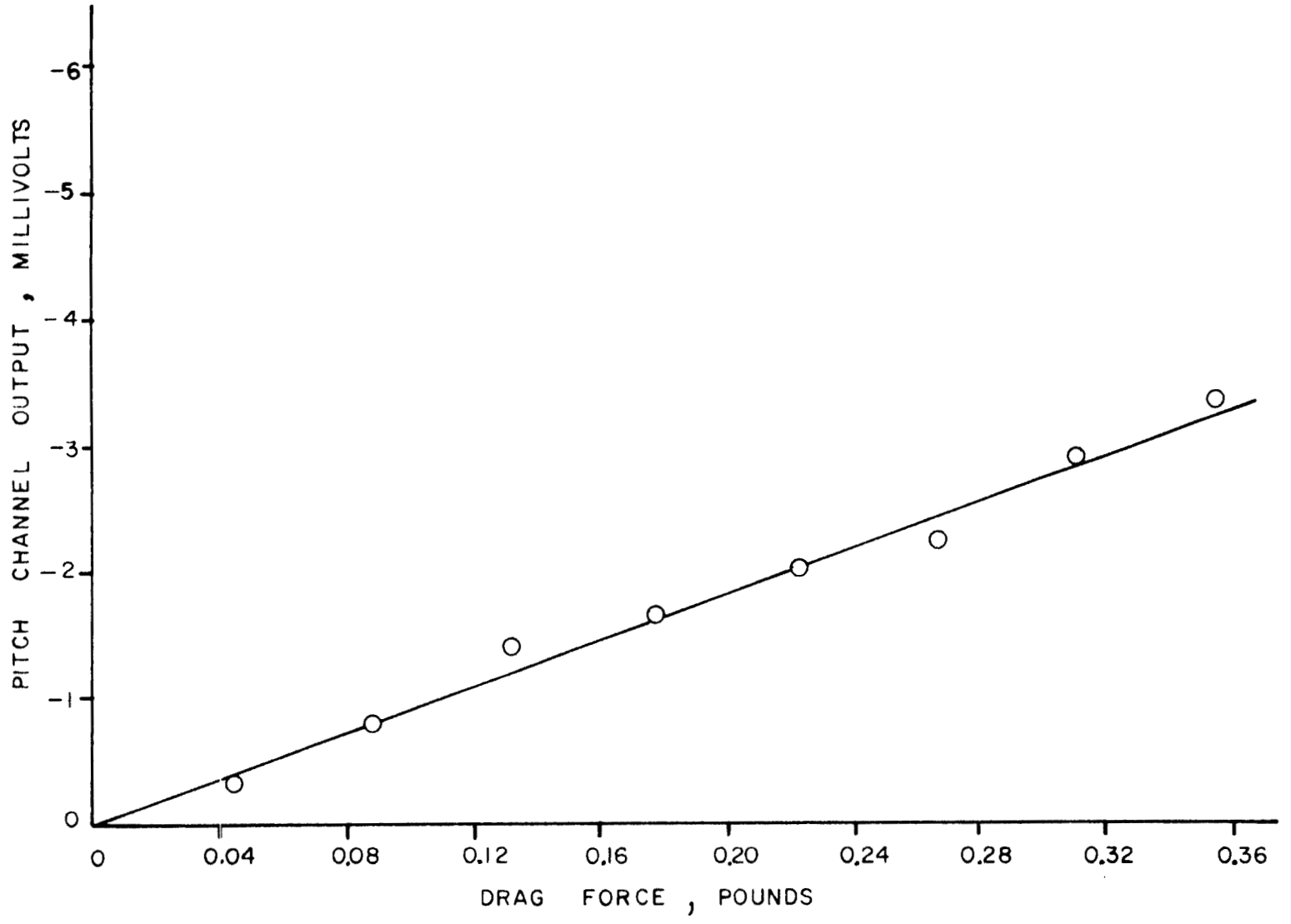

FIGURE 34 PITCH CHANNEL OUTPUT VS - DRAG FORCE

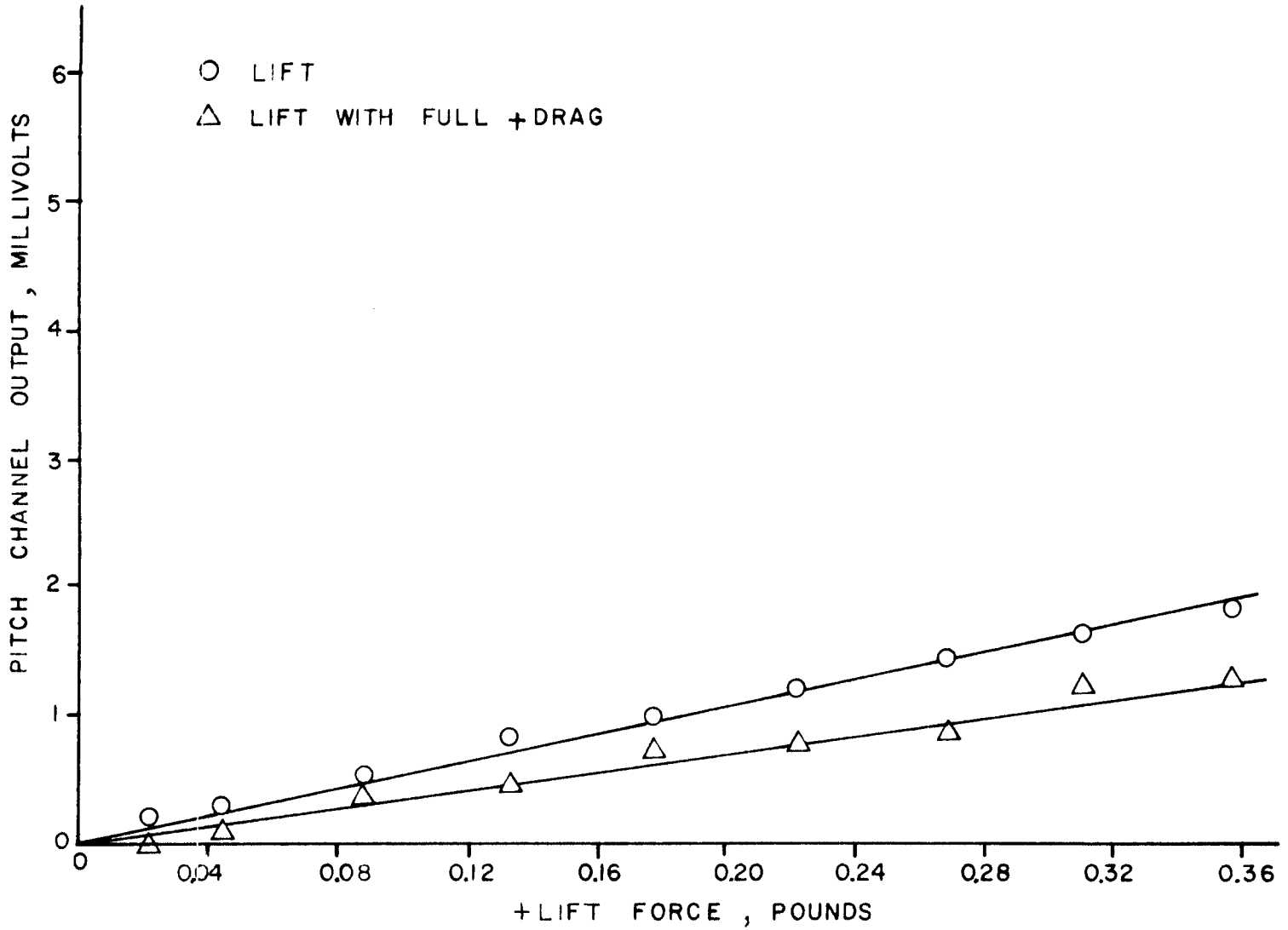

FIGURE 35 PITCH CHANNEL OUTPUT VS + LIFT FORCE

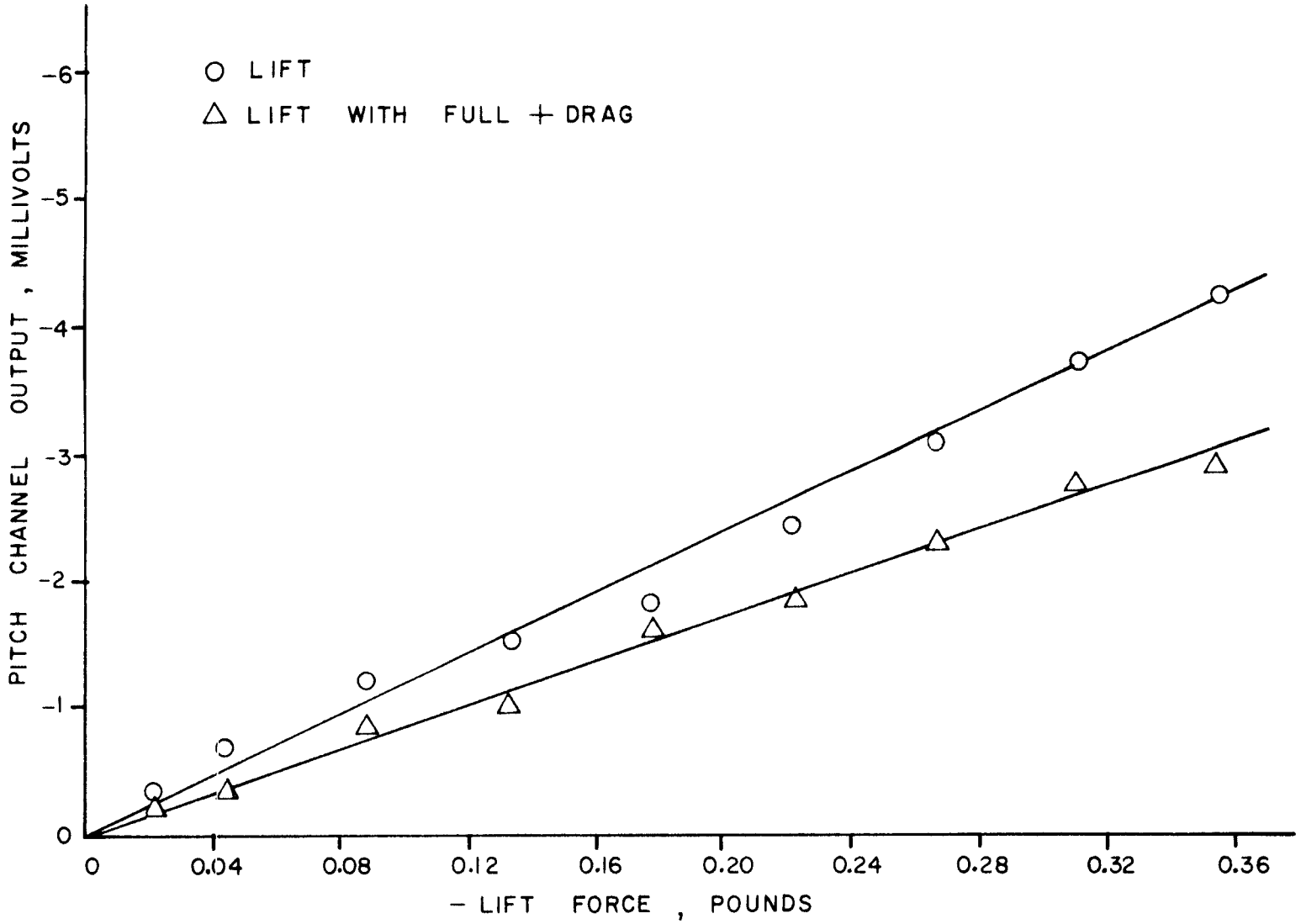

FIGURE 36 PITCH CHANNEL OUTPUT VS - LIFT FORCE

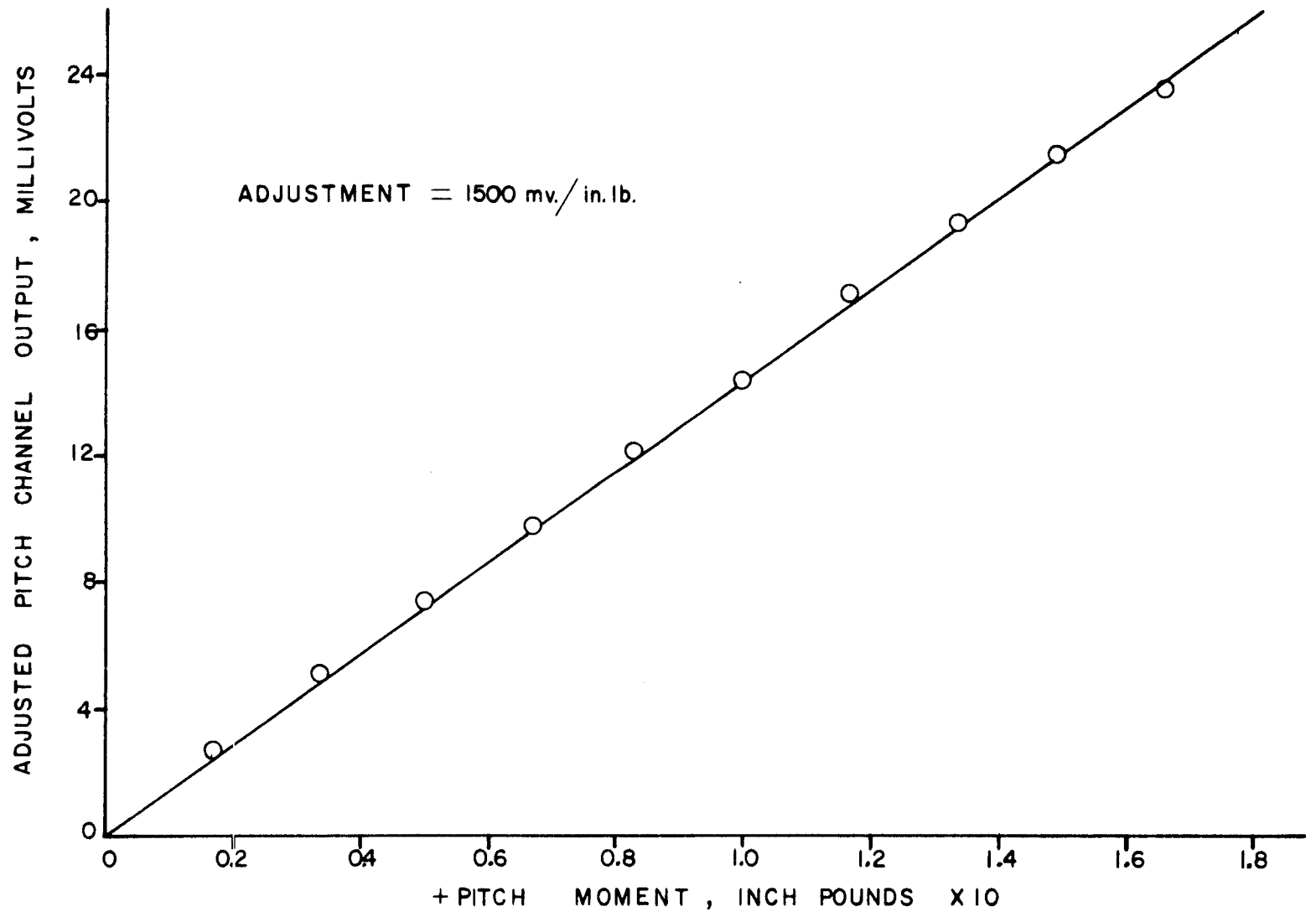

FIGURE 37 PITCH CHANNEL OUTPUT VS + PITCH MOMENT, LOW RANGE

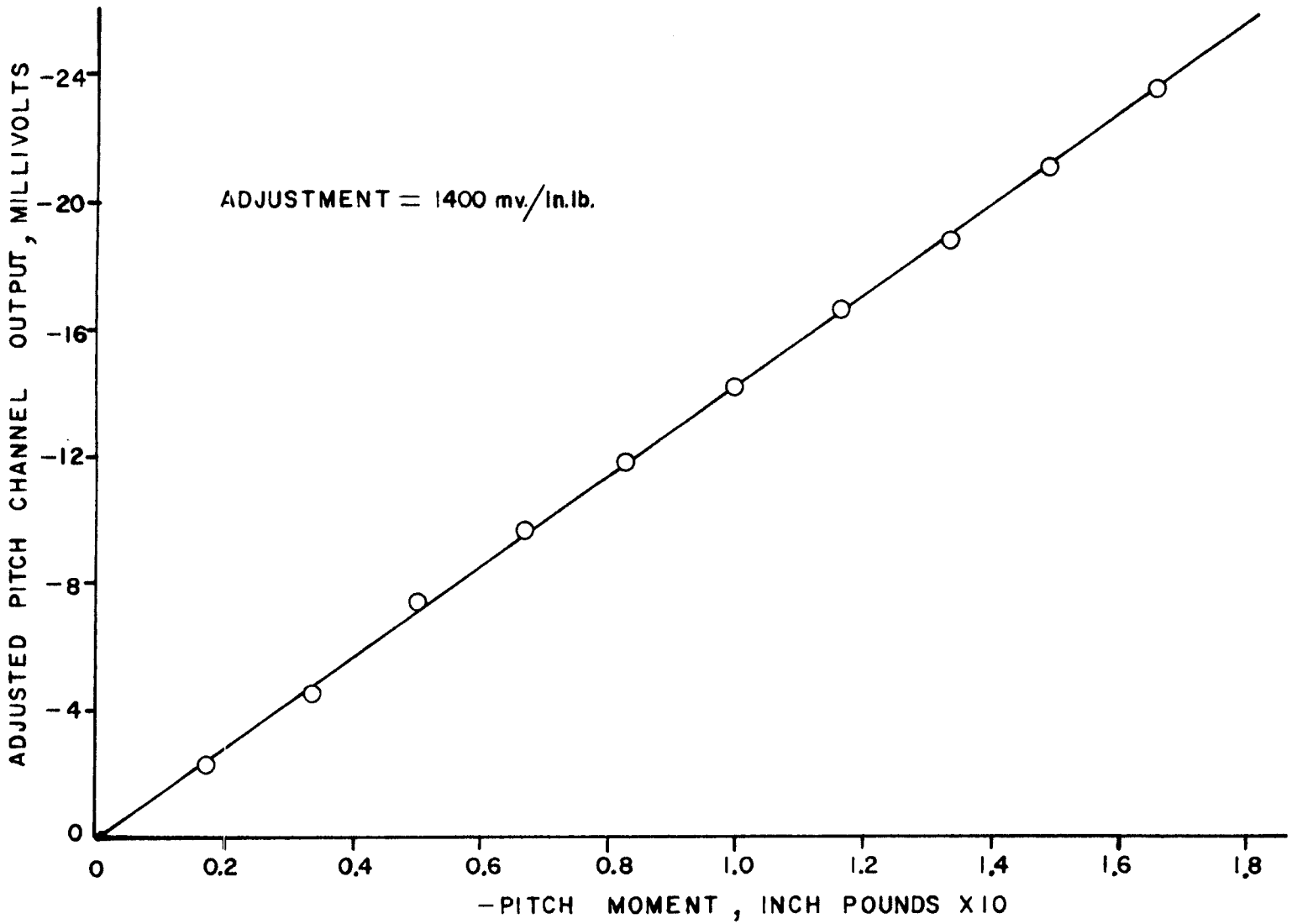

FIGURE 38 PITCH CHANNEL OUTPUT VS - PITCH MOMENT, LOW RANGE

$$k_{DDL} = \frac{\theta_{DDL}}{\text{Drag x Lift}} \times k_{DD} = \frac{\theta_{DDL}}{DXL} \times k_{DD} = \frac{4.2 \text{ mv}}{(.3600\#)(.3600\#)}$$

$$\times 4.155 \times 10^{-4} \#/\text{mv}$$

$$k_{DDL} = +1.3465 \times 10^{-2}/\#$$

Determination of k_{DDM}. Curves D and E of Figure 19 are plots of the drag channel output for applied drag load with full positive and negative pitch moment respectively. This is a positive interaction since positive pitch causes the positive drag load curve to shift upward to a higher value for a given load. The shift of curves D and E from A at a drag load of 0.3600# is + 3.0 mv and - 1.6 mv respectively. The average magnitude of the shift is θ_{DDM} where

$$\theta_{DDM} = \frac{3.0 + 1.6}{2} = 2.3 \text{ mv}$$

$$\therefore k_{DDM} = \frac{\theta_{DDM}}{\text{Drag x Pitch}} \times k_{DD} = \frac{\theta_{DDM}}{D \times M} \times k_{DD} =$$

$$k_{DDM} = \frac{2.3 \text{ mv}}{(.3600\#)(1.800 \text{ inch \#})} \times 4.155 \times 10^{-4} \#/\text{mv} = 1.4748 \times 10^{-3}/\text{inch\#}$$

Determination of k_{DLM}. In Figure 20, curves B and C are plots of drag channel output for positive lift loads with full positive and negative applied pitching moment. Similarly, curves B and C of Figure 21 are plots of drag channel output for negative lift loads with full positive and negative applied pitching moments. The shift of curves B and C from curve A (pure lift load) is due to cross product coupling and is proportional to the product of lift and pitch. This interaction is positive since a positive lift load with a positive pitch moment produces a positive drag channel output signal. The average shift of curves B and C from A is θ_{DLM} where

$$\theta_{DLM} = \frac{1.15 + .85 + .875 + .90}{4} = 0.94 \text{ mv}$$

$$k_{DLM} = \frac{\theta_{DLM}}{\text{Lift x Pitch}} \times k_{DD} = \frac{\theta_{DLM}}{L \times M} \times k_{DD} = \frac{0.94 \text{ mv}}{(.360\#)(1.80 \text{ inch \#})} \times 4.155 \times 10^{-4} \#/\text{mv}$$

$$k_{DLM} = 6.0273 \times 10^{-4}/\text{inch-pound.}$$

Table III gives the determination of calibration equation coefficients for the drag channel for the 0.5# range in condensed form. Column #1 gives the calibration coefficient to be determined. Column #2 lists the load term, or terms, involved and column #3 is the actual value or values of these terms. Column #4 lists the full scale effect of the term in milli-volts. Column #5 is the quotient of the output signal over the load term, or terms, $(\frac{\text{column \#4}}{\text{column \#3}})$. Column # 6 contains the product of column # 5 and the sensitivity constant k_{DD}, and is the actual value of the calibration coefficient. Column #7 lists the percentage of the terms of full scale value.

Tables IV, V, VI, and VII were calculated using the same procedure as was used to determine the drag calibration coefficients. Tables IV and V contain the calibration coefficients for the positive and negative lift channels respectively. Tables VI and VII contain the calibration coefficients for positive and negative pitch channels respectively.

Table VIII lists the sensitivity constants for the drag, lift and pitch channels for the 0.05# ranges. As stated before, no determination of cross coupling effects was made for this range.

FINAL CALIBRATION EQUATIONS

The following equations are used to determine the unknown forces applied to the system from the output signals of the three readout channels.

TABLE III

DRAG CALIBRATION EQUATION COEFFICIENTS

① Calibration Coefficient	② Load Term or Terms	③ Value of Load Terms	④ Average Value of Effect	⑤ ④ / ③	⑥ ⑤ x Sensit. Constant	⑦ % of Full Scale
-	-	pounds inch-pounds	mv	mv/pound mv/inch-pound	-	-
k_{DD}	D	0.3600#	+ 866.5	-	$+4.155 \times 10^{-4}$	-
k_{DL}	L	0.3600#	+ 1.75	4.8611	$+2.0197 \times 10^{-3}$	0.2
k_{DM}	M	1.800 in #	+ 6.3	3.500	$+1.4542 \times 10^{-3}$	0.7
k_{DD^2}	D^2	(.3600)(.3600)	≈ 0	-	-	-
k_{DL^2}	L^2	(.3600)(.3600)	≈ 0	-	-	-
k_{DM^2}	M^2	(1.800)(1.800)	≈ 0	-	-	-
k_{DDL}	D x L	(.3600)(.3600)	+ 4.2	32.407	$+1.346 \times 10^{-2}$	0.5
k_{DDM}	D x M	(.3600)(.3600)	+ 2.3	3.549	$+1.475 \times 10^{-3}$	0.3
k_{DLM}	L x M	(.3600)(.3600)	+ .94	1.451	$+6.027 \times 10^{-4}$	0.1

TABLE IV

+ LIFT CALIBRATION EQUATION COEFFICIENTS

① Calibration Coefficient	② Load Term or Terms	③ Value of Load Term	④ Average Value of Effect	5) ④/③	⑥ ⑤x k_{LL}	7 % of Full Scale
-	-	pounds inch-pounds	mv	mv/pounds mv/inch-pounds	-	-
k_{LL}	L	0.360	+ 813.4	-	$+4.427 \times 10^{-4}$	-
k_{LD}	D	0.360	+ 5.0	+ 13.888	$+6.148 \times 10^{-3}$	0.6
k_{LM}	M	1.800	- 1.8	- 1.000	-4.427×10^{-4}	0.2
k_{LL^2}	L^2	(.360)(.360)	≈ 0	-	-	-
k_{LD^2}	D^2	(.360)(.360)	≈ 0	-	-	-
k_{LM^2}	M^2	(1.80)(1.80)	≈ 0	-	-	-
k_{LLD}	L x D	(.360)(.360)	- 4.0	- 30.8669	-1.366×10^{-2}	0.5
k_{LDM}	D x M	(.360)(.360)	- 1.40	- 2.16049	-9.564×10^{-4}	0.2
k_{LLM}	L x M	(.360)(.360)	+ 2.6	+ 4.0123	$+1.776 \times 10^{-3}$	0.3

TABLE V

- LIFT CALIBRATION EQUATION COEFFICIENTS

1	②	3	④	⑤	⑥	⑦
Calibration Coefficient	Load Term or Terms	Value of Load Term	Average Value of Effect	④ / ③	⑤ x k_{LL}	% of Full Scale
-	-	pounds inch-pounds	mv	mv/pound mv/inch-pound	-	-
k_{LL}	L	0.360	776.0	-	$+4.639 \times 10^{-4}$	-
k_{LD}	D	0.360	+ 5.0	+ 13.889	$+6.443 \times 10^{-3}$	0.6
k_{LM}	M	1.800	- 1.8	- 1.000	-4.639×10^{-4}	0.2
k_{LL^2}	L^2	(.360)(.360)	≈ 0	-	-	-
k_{LD^2}	D^2	(.360)(.360)	≈ 0	-	-	-
k_{LM^2}	M^2	(1.80)(1.80)	≈ 0	-	-	-
k_{LLD}	L x D	(.360)(.360)	- 2.4	- 18.518	-8.591×10^{-3}	0.3
k_{LDM}	D x M	(.360)(.360)	- 1.40	- 2.1605	-1.002×10^{-3}	0.2
k_{LLM}	L x M	(.360)(.360)	+ 4.5	+ 6.9444	$+3.222 \times 10^{-3}$	0.6

TABLE VI

+ PITCH CALIBRATION EQUATION COEFFICIENTS

① Calibration Coefficient	② Load Term or Terms	③ Value of Load Term	④ Average Value of Effect	⑤ ④ / ③	⑥ ⑤ x k_{MM}	⑦ % of Full Scale
-	-	pounds inch-pounds	mv	mv/pounds mv/inch-pounds	-	-
k_{MM}	M	1.800	380.2	-	$+4.734 \times 10^{-3}$	-
k_{ML}	L	0.360	+ 3.1	+ 8.611	$+4.077 \times 10^{-2}$	0.8
k_{MD}	D	0.360	- 3.3	- 9.167	-4.340×10^{-2}	0.9
k_{MM^2}	M^2	(1.80)(1.80)	≈ 0	-	-	-
k_{ML^2}	L^2	(.360)(.360)	≈ 0	-	-	-
k_{MD^2}	D^2	(.360)(.360)	≈ 0	-	-	-
k_{MMD}	M x D	(1.80)(.360)	- 1.6	- 2.469	-1.169×10^{-2}	0.4
k_{MML}	M x L	(1.80)(.360)	- 1.8	- 2.778	-1.315×10^{-2}	0.5
k_{MDL}	D x L	(.360)(.360)	- .9	- 6.944	-3.288×10^{-2}	0.2

TABLE VII

- PITCH CALIBRATION EQUATION COEFFICIENTS

① Calibration Coefficient	② Load Term or Terms	③ Value of Load Term	④ Average Value of Effect	⑤ ④ / ③	⑥ 5 x k_{MM}	7 % of Full Scale
-	-	pounds inch-pound	mv	mv/pounds mv/inch-pound	-	-
k_{MM}	M	1.800	362.2	-	$+4.9696 \times 10^{-3}$	-
k_{ML}	L	0.3600	+ 3.1	+ 8.611	$+4.279 \times 10^{-2}$	0.9
k_{MD}	D	0.3600	- 3.3	- 9.167	-4.556×10^{-2}	0.9
k_{MM^2}	M^2	(1.80)(1.80)	≈ 0	-	-	-
k_{ML^2}	L^2	(.360)(.360)	≈ 0	-	-	-
k_{MD^2}	D^2	(.360)(.360)	≈ 0	-	-	-
k_{MMD}	M x D	(1.80)(.360)	- 1.5	- 2.315	-1.150×10^{-2}	0.4
k_{MML}	M x L	(1.80)(.360)	- 2.0	- 3.086	-1.534×10^{-2}	0.6
k_{MDL}	D x L	(.360)(.360)	- .9	- 6.944	-3.451×10^{-2}	0.2

TABLE VIII

SENSITIVITY CONSTANTS FOR LOW RANGES

Calibration Coefficients	Load Term	Load Value	Adjustment Constant	Adjustment	Adjusted Output	Total Output	Sensitivity Constant
-	-	pounds inch-pounds	mv/pound mv/inch-pound	mv	mv	mv	pounds/mv inch-pound/mv
k_{DD}	+ Drag	+0.036#	+ 25,800	+928.8	+ 26.6	+955.4	3.768×10^{-5}
k_{LL}	+ Lift	+0.0360#	+ 22,500	+810.0	+ 27.8	+837.8	4.297×10^{-5}
k_{LL}	- Lift	-0.0360#	+ 21,500	-774.0	- 14.4	-788.4	4.566×10^{-5}
k_{MM}	+ Pitch	+0.180 inch#	+ 1500	+270.0	+ 25.7	+295.7	6.087×10^{-4}
k_{MM}	- Pitch	-0.180 inch#	+ 1400	-252.0	- 25.4	-277.4	6.489×10^{-4}

Low Range. The output signals θ_D, θ_L, and θ_M are expressed in units of millivolts. The drag and lift forces are in units of pounds and the pitching moments are in units of inch-pounds.

$$\text{Drag Force } D = (3.768 \times 10^{-5}) \times \theta_D$$
$$+ \text{ Lift Force } L = (4.297 \times 10^{-5}) \times \theta_L$$
$$- \text{ Lift Force } L = (4.566 \times 10^{-5}) \times \theta_L$$
$$+ \text{ Pitch Moment } M = (6.087 \times 10^{-4}) \times \theta_M$$
$$- \text{ Pitch Moment } M = (6.489 \times 10^{-4}) \times \theta_M$$

High Range. The forces determined below are uncorrected and as such contain errors due to direct and cross product coupling between measurement channels. The output signals are expressed in units of millivolts, the drag and lift forces in pounds, and the pitching moments expressed in inch pounds.

$$\text{Drag Force } D_0 = (4.155 \times 10^{-4}) \times \theta_D$$
$$+ \text{ Lift Force } L_{0_+} = (4.427 \times 10^{-4}) \times \theta_L$$
$$- \text{ Lift Force } L_{0_-} = (4.639 \times 10^{-4}) \times \theta_L$$
$$+ \text{ Pitch Moment } M_{0_+} = (4.734 \times 10^{-3}) \times \theta_M$$
$$- \text{ Pitch Moment } M_{0_-} = (4.970 \times 10^{-3}) \times \theta_M$$

The above uncorrected forces D_0, L_0 and M_0 are inserted into the calibration equations below to solve for the correct, adjusted values of unknown forces and pitching moment. The terms within the brackets are the correction terms to adjust for the cross coupling effects. Normally, the algebraic sum of these corrections will be 1% or less of the full scale value of the load component to be measured.

$$D = D_0 - [(2.020 \times 10^{-3}) \times L_0 + (1.454 \times 10^{-3}) \times M_0 + (1.346 \times 10^{-2})$$
$$\times D_0 \times L_0 + (1.475 \times 10^{-3}) \times D_0 \times M_0 + (6.027 \times 10^{-4}) \times L_0 \times M_0]$$

$$+L = L_{0_+} - [(6.148 \times 10^{-3}) \times D_0 - (4.427 \times 10^{-4}) \times M_0 - (1.366 \times 10^{-2}) \times L_{0_+} \times D_0 - (9.564 \times 10^{-4}) \times D_0 \times M_0 + (1.776 \times 10^{-3}) \times L_{0_+} \times M_0]$$

$$-L = L_{0_-} - [(6.443 \times 10^{-3}) \times D_0 - (4.639 \times 10^{-4}) \times M_0 - (8.591 \times 10^{-3}) \times L_{0_-} \times D_0 - (1.002 \times 10^{-3}) \times D_0 \times M_0 + (3.222 \times 10^{-3}) \times L_{0_-} \times M_0]$$

$$+M = M_{0_+} - [(4.077 \times 10^{-2}) \times L_0 - (4.340 \times 10^{-2}) \times D_0 - (1.169 \times 10^{-2}) \times M_{0_+} \times D_0 - (1.315 \times 10^{-2}) \times M_{0_+} \times L_0 - (3.288 \times 10^{-2}) \times D_0 \times L_0]$$

$$-M = M_{0_-} - [(4.279 \times 10^{-2}) \times L_0 - (4.556 \times 10^{-2}) \times D_0 - (1.150 \times 10^{-2}) \times M_{0_-} \times D_0 - (1.534 \times 10^{-2}) \times M_{0_-} \times L_0 - (3.451 \times 10^{-2}) \times D_0 \times L_0]$$

DESCRIPTION OF SYSTEM OUTPUT DATA

Hysteresis. For each loading trial, the weights were loaded in positive increments from zero to full load and then in negative increments back to zero load. A preliminary run indicated a small amount, (1 - 2%) of hysteresis but this was found to be due to friction between the LVDT cores and their respective transformer coil walls. Careful realignment reduced this hysteresis to a point where it was not distinguishable from the background vibration noise. It is therefore concluded that the hysteresis of the system is of a negligible magnitude as far as its effect on force measurement is concerned.

Scatter of Output Data. Three loading trials were made for each load combination on the high range and five were made for the low force range. The variations between trials for the high range were as follows.

Lift Channel Scatter = ± 0.6 mv = ± 0.1% of Full Scale
Drag Channel Scatter = ± 0.6 mv = ± 0.1% of Full Scale
Pitch Channel Scatter = ± 0.2 mv = ± 0.07% of Full Scale

For the low range, the output signal was found to have fluctuations of approximately ±5 mv on the drag and lift channels and approximately ±3 mv on the pitch channel. When reading the output signal, an effort was made to read the middle value approximately half way between the upper and lower boundaries of these fluctuations. These averaged values for each trial were then averaged again and the individual readings were found to be within ±2 mv of the average value.

It is believed that most of the above output signal scatter was due to the background vibration effects. Proper vibration isolation would reduce this effect significantly. Another possible way to reduce this output signal scatter would be to use proper output filtering. An output filter with a slow response time (1 or 2 seconds) would allow a time averaged output signal without much influence from the higher frequency fluctuations.

Scatter of Plotted Values. The expanded scale calibration plots give a good measure of the scatter of the averaged values of the output signal. The high range (0.5 #) measurements indicate a point to point scatter of no more than ± 1.5 mv out of a full scale value of 775 mv from the assumed straight line for drag and lift. This corresponds to a scatter of less than ± 0.2% of the full scale value. The pitch variations were less than ± 0.5 mv out of a full scale value of 350 mv which corresponds to a scatter of ± 0.14% from the assumed straight line plot.

The scatter of the plotted averaged values is approximately twice that of the variations between trials for each load increment. It is therefore concluded that the scatter of the plotted averaged values is due to random variations in the calibration forces and moments rather than the system itself.

CHAPTER VI
ANALYSIS OF CALIBRATION ERRORS

CALIBRATION FORCE MAGNITUDE ERRORS

Calibration Weights. The calibration balance and string force devices were loaded with precision analytical balance brass weights. The weights were National Bureau of Standards class S--1 gram weight sets and were readily available from the Mechanical Engineering Department's student laboratories. These weights have a tolerance of ± 0.01%[9] and were used exclusively on all loadings except for the maximum load, (.3527#), applied to the drag and lift components. For the maximum drag and lift loading, three brass 100 gram calibration weights were made in the Mechanical Engineering Department's machine shop. These were made of round brass bar stock and were machined to a size suitable for balance loading. These weights were weighed with a Mettler H-15 substitution balance to the nearest 0.1 mg and four separate trials were run for each of the weights. Averages of the trials indicated that the three weights were all within a tolerance range of ± 0.015 gm. Therefore, the error in using these specially made weights was $\frac{\pm 0.015 \text{ gm}}{100 \text{ gm}} \times 100 = \pm 0.015\%$. The weights were checked three times during the calibration procedure and no appreciable variation in their weight was detected.

Balance Arm Ratio Errors. The horizontal and vertical beams of the calibration balance were measured with vernier calipers to determine the magnitude ratio for the balance. As stated before, the balance was designed to provide a horizontal calibration force of two-thirds the weight of the calibration weights applied to the balance pan.

---

[9] T. W. Lashof and L. B. Macurdy, "Precision Laboratory Standards of Mass and Laboratory Weights." Washington, D. C: United States National Bureau of Standards, Circular 547, Section 1, August 20, 1954.

The lengths of the two beams were measured to the nearest two-one thousandths of an inch. The horizontal beam was found to be 3.000 ± 0.002" long and the vertical beam to be 4.500 ± 0.002" long. Thus, the possible range of ratios for the two beams would be $R = \frac{3.000 \pm 0.002}{4.500 \pm 0.002}$. The percentage error in the applied force due to this ratio uncertainty is $(\frac{\pm 0.002}{3.000} + \frac{\pm 0.002}{4.500}) \times 100 = \pm 0.12\%$.

Balance Force Application Errors. Figure 39 illustrates the method used to transfer the force from the calibration balance to the sting. It had originally been planned to let the vertical beam of the balance push against the sting via a pointed contact pin. However, it was found that friction effects between the contact pin and sting were too great to allow reliable calibration data. The steel ring and thread arrangement eliminated this problem of friction but introduced another source of error, that of non horizontal force application to the sting. The thread and ring were adjusted to a horizontal position, (perpendicular to sting and vertical beam of balance) by adjustment of the heighth of the ring. It is estimated that variations in h were limited to a range of ± 0.0625". Thus the maximum possible angle of inclination α of the applied load would be $\alpha = \tan^{-1}(\frac{\pm h}{c}) = \tan^{-1}(\frac{\pm 0.0625}{1.25}) = \tan^{-1}(\pm 0.050) = \pm 2.83°$. The actual horizontal calibration force applied to the sting is $P \cos \alpha = P \cos(\pm 2.83°) = \pm P(0.9988)$. The percentage error due to such an inclimation is $\pm(\frac{1-0.9988}{1}) \times 100 = \pm 0.12\%$.

Balance Friction Effects. The knife edge friction of the balance was determined as explained in the section on balance performance check of Chapter 4. As shown in Figure 10, the effect of this friction on the calibration force varies with the applied load. The balance was limited to loads larger than 0.05# which would limit the percentage error of applied calibration force due to knife edge friction to less than ±0.2% error. For the larger loads, the error is even less. Therefore, the maximum error due to knife edge friction is ± 0.2% of the applied load.

String Force Device Errors. As stated in Chapter 4, the accuracy of the calibration load obtained with the string force device is only limited by the precision of the weights and the precision of measurement

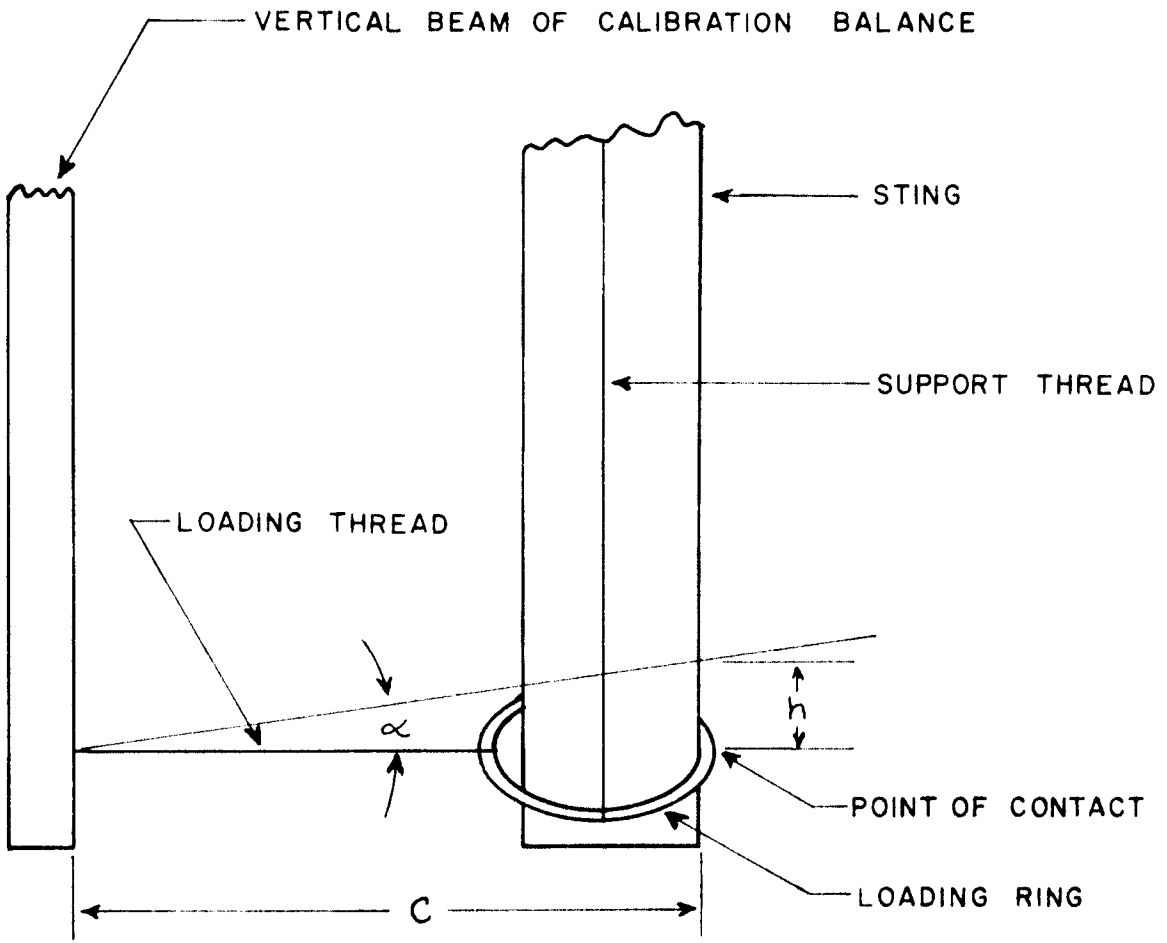

FIGURE 39 LOADING RING ARRANGEMENT

of lengths a and b. The horizontal force component (calibration load) is equal to W $(\frac{a}{b})$. Both a and b can be held to a tolerance of ± 1/32". This produces a possible calibration force (P) = W $(\frac{12 \pm 1/32}{24 \pm 1/32})$ letting a = 12.03125" and b = 23.96875" gives a/b = 0.501955.

$$\% \text{ Error} = \pm \left(\frac{.501955 - .50000}{.50000}\right) \times 100 = \pm 0.391\% \text{ Max Error}$$

Pitch Moment Arm Length Errors. The calibration pitch moments were produced by applying positive drag at Z = ± 15" from the center of the bottom of the sting. The length of the moment arm was found to be accurate within ± 1/32. The error introduced by considering the length to be exactly 15" is the following. Error = $(\frac{15 \pm 1/32 - 15}{15}) \times 100$ = ± 0.208%.

CALIBRATION FORCE MISALIGNMENT ERRORS

Rotary Table Angle Errors. The calibration balance was mounted on a machinist's rotary table to turn off horizontal loading angles. The rotary table had a least count of 0.1° and checks indicated its accuracy to be at least this good. Figure 16 illustrates the effect of the uncertainty of ψ on the calibration data. Assume positive drag is loaded at ψ = -.75 and that ψ has an uncertainty $\Delta\psi$ of ± 0.10°. The actual drag load will be P cos $\Delta\psi$ = P cos (±0.10°) = P (1.000) = P. The orthogonal loading, (lift), introduced by $\Delta\psi$ will be P sin $\Delta\psi$ = P sin (± 0.10) = P (± 0.0017)= 0.17% of P. Therefore, a full drag load could apply a maximum lift load of 0.17% of full load. This component would appear as a cross coupling effect while it would actually be an applied lift load. The load applications using the string force devices were held to a similiar tolerance and thus the upper limit on orthogonal loading would be 0.17% of full load capacity.

Errors due to Offset of Sting. It was found that the sting had a permanent bend in it which produced an offset (δ) of the center of the bottom of the sting with respect to the center of the measurement system at the top. This offset was found to be approximately 1/16". When assembling the system an attempt was made to line up the sting so that this offset was pointed in the -X direction. Since all calibration loads

were applied at the bottom of the sting, they were not actually applied at the true center of the force measurement system. Figure 40 illustrates the effect of this offset on the system calibration loading. Due to an offset in a -X direction, positive and negative lift calibration loads actually apply a pitch moment to the system of magnitude equal to the lift load times the offset. Thus, a full positive lift load of 0.3527# would also apply a pitch moment of $L\delta = (0.3527)(0.0625) = 0.0220$ inch pounds. The full load pitch moment is 1.6538 inch pounds and thus the percentage of lift-induced pitch is $\frac{0.0220}{1.6538} \times 100 = 1.33\%$ of full pitch moment.

The calibration data indicated a cross coupling effect between lift loads and the pitch channel output signal of a magnitude similiar to the above. It was found that the application of positive full lift caused a pitch channel signal of + 0.8% of full scale while the above analysis indicates it should be + 1.33% assuming no cross coupling. Differences between the two may be due to one or both of two causes. First, the difference may be due to a negative cross coupling effect between lift and pitch which reduces the actual lift produced pitch channel signal. Or, the difference may be due to misalignment errors and force magnitude errors of the calibration forces. Since the difference is of approximately the same magnitude as the possible misalignment and magnitude errors of the applied force, it is not possible to determine which is the predominent cause.

It is therefore reasonable to assume that the cross coupling effects of applied lift load on pitch readout are partly due to this offset. Since the overall system including the sting was to be calibrated, no allowance was made for this sting offset in the determination of cross coupling coefficients. Had the offset been lined up with the ± Z direction, an applied drag load would produce a similiar pitch moment on the system. In addition to this effect, an offset in the ± Z direction would move the center of the pitch application moment arm away from the true center of the system. Thus, one pitch arm would have a length of 15" + offset (δ) and the other a length of 15" - offset (δ). Equal loads on each end of

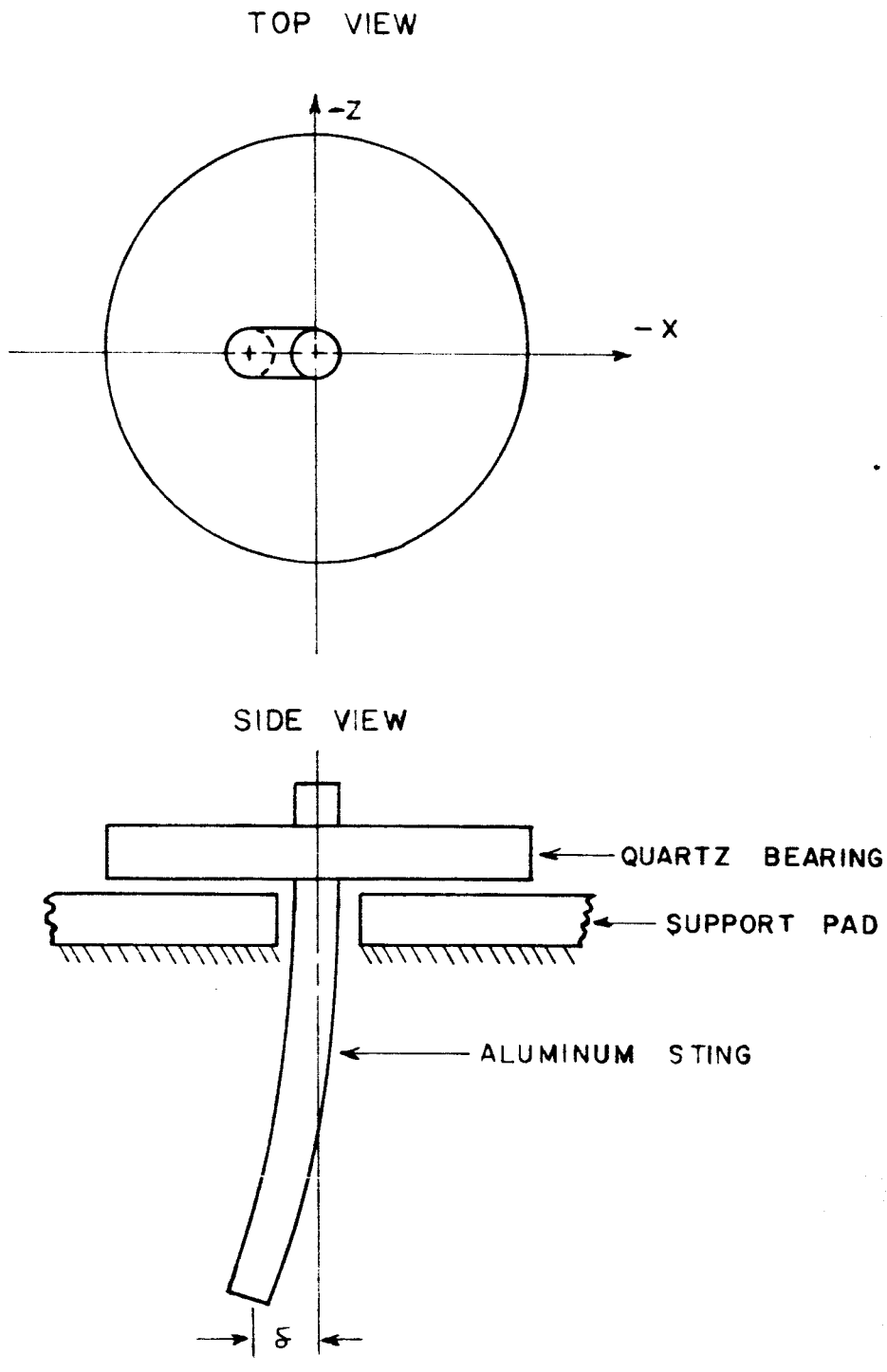

FIGURE 40 STING OFFSET

the pitch arm would produce unequal positive and negative pitch moments on the system. As an example let the offset be 0.125". Then the pitch magnitude variation would be:

$$\Delta M = \frac{15.125 - 14.875}{15.000} = 0.0167 = 1.67\% \text{ Variation.}$$

Thus, the readout signals due to apparently equal applied positive and negative pitching moments would vary by 1.67%.

It should therefore be pointed out that the calibration of the system is relatively sensitive to the magnitude and direction of sting offset. Thus, a different sting with different offset would change the calibration constants for the system.

ERRORS DUE TO READOUT EQUIPMENT

As stated before, all readout signal measurements were made with a DANA series 5600 digital volt meter. This instrument has an accuracy of ± 0.001% of full scale for each range. All readings were made on the 1 volt range so that the accuracy was ± 0.001% of 1 volt or ± 0.01 mv. The readout signals were only read to the nearest tenth of a mv and thus the readout meter has an accuracy one whole order of magnitude better than required. Therefore, the readout error due to the digital volt meter need not be considered.

PLOTTING AND DATA REDUCTION ERRORS

The output data was originally plotted on 25 cm x 38 cm graph paper. The expanded scale plotting technique allowed the output voltages to be plotted to the nearest ± 0.1 mv and the applied drag and lift loads to the nearest ± 0.002# on the 0.5# range and ± 0.0002# on the 0.05# range. The pitching moments were plotted to the nearest ± 0.01 inch pound on the 2.0 inch-pound range and ± 0.001 inch-pound on the 0.2 inch-pound range. The plotting precision is therefore the same for the high and low ranges and is the following.

Voltage scale precision = $\frac{\pm 0.1 \text{ mv}}{775} \times 100 = \pm 0.13\%$ of Full Scale

Drag and Lift load scale precision = $\frac{\pm 0.002}{0.3600} \times 100 = \pm 0.55\%$ of Full Scale

Pitching moment scale precision = $\frac{\pm 0.01}{1.80} \times 100 = \pm 0.55\%$ of Full Scale

As discussed in Chapter V, the digital computer was used to fit a first order polynomial to the output data using a least squares error curve fit. It was found that the slope of the line given by the expanded scale plotting technique agreed within ± 0.1% of that given by the computer fit.

CHAPTER VII
EFFECTS OF AMBIENT CONDITIONS ON SYSTEM

Room Temperature. The laboratory in which the calibration was done is air conditioned and was kept within a temperature range of 71° to 73°F. A thermometer was placed near the system and the temperature observed for each run. No noticable effects on the system were observed for temperature fluctuations within this 71° to 73°F range.

Warmup and Drift of Electronic Equipment. All of the electronic equipment except for the solid state control amplifiers was turned on at least eight hours before any calibration run to allow for proper warm up. The air bearing was floated and the solid state control amplifiers turned on at least 15 minutes before any calibration runs to insure proper warm-up. However, no noticable difference was found between results after 15 minutes of warmup and those with no warmup allowance.

Room Air Currents. During calibration runs, an effort was made to reduce stray air currents around the system to a minimum. A plastic dust cover had been made to cover the air bearings and control motors and this was left in place during calibration runs. In addition, a series of cardboard baffles were placed around the support base to isolate the sting and calibration balance from stray air currents. The laboratory air conditioning system was turned off during the calibration runs to reduce the air currents. It was found that for extended calibration runs a fan was necessary to force cool the power transistors of the control amplifiers. A check was made to determine the effect on the system of the air currents created by this fan. No measurable difference between output readings with the fan and those without it was noticed.

Air Bearing Flutter. During the first few calibration runs a slight audible flutter was detected in the air bearing. The bearing was disassembled and thoroughly cleaned to remove any foreign matter entrapped in the oriffices. Upon reassembly of the bearing, it was found that the flutter was still present but to a lesser degree. After several more cleanings didn't eliminate the flutter, it was decided to make the calibration runs with it present.

An attempt was made to determine the effect of this flutter on the system performance. The control loop was broken and the LVDT output of the non-servoed system observed on an oscilloscope for various main pad and holddown pad pressures. With the bearing in the floated position, the LVDT sensors Z_1 and Z_2 were found to have a randomly varying output signal ripple of approximately ±0.3 mv. The signal was found to have frequencies within the 1 cps to 5 cps range and a most predominant frequency of approximately 4 cps. The pad pressures were varied between 4 and 40 psi and only slight, (5 - 10%), changes in the LVDT output signals were noted indicating the air bearing flutter to be a minor cause of the bearing vibrations. It was found that the audible flutter of the bearing was a minimum at pressures of 8 psi for the main pad and 18 psi for the hold down bearings. These pressures were maintained for all of the calibration runs.

Background Vibrations. It is believed that background vibrations of the system support base were the major cause of the LVDT output variations mentioned above. With the bearing floated, the system would act as a vibration sensitive pickup with the bearing glass-sting assembly acting as the vibratory body and the LVDT acting as the electrical sensor. The vibrations were found to have a predominant frequency of 4 cps. Hicks in an earlier study of the vibratory characteristics of the support base observed similiar background vibrations of approximately 4 cps[10]. It is believed that proper isolation of the bearing system from the support base with a vibration damping material such as Isomode would greatly reduce the effect of background vibrations on system performance. Lack of time however, prevented a complete analysis of this effect.

---

[10]Hicks, op. cit., pp. 103-107.

CHAPTER VIII
CONCLUSIONS AND RECOMMENDATIONS

CONCLUSIONS

As a result of the foregoing study, the following conclusions were reached.

1. The calibration equipment and technique provide the desired force measurement system performance data.

2. The force measurement system was found to have less than 1% cross coupling between channels as predicted by an earlier theoretical analysis. The force measurement system was found to be suitable for wind tunnel model testing.

3. The ultimate sensitivity and precision of the system were found to be limited by the influence of the background vibrations of the support base.

4. It is believed that the ultimate lower limit on the useful measurement range of the system will be determined by the calibration equipment and procedure rather than the system itself.

RECOMMENDATIONS

The following recommendations are made as possible areas for future study.

A. Suggested Improvements in Calibration Equipment. The precision of the calibration balance loads was limited by knife edge friction. For this reason, the string force devices or a similiar arrangement would be the best approach for future design efforts since they eliminate error causing friction.

B. Suggested Improvements in Force Measurement System.

1. One of the first problem areas to be investigated should be that of proper isolation of the system from background vibrational input.
2. The mountings for the LVDT sensors should be redesigned to

provide more accurate position adjustments.

3. Mechanical stops should be installed to prevent the LVDT cores from banging against the transformer coils during turn-on transients.

BIBLIOGRAPHY

Arney, G. D., Jr. and Wade T. Harter. "A Low-Load Three-Component Force Balance for Measurements in a Low-Density Wind Tunnel." International Congress on Instrumentation in Aerospace Simulation Facilities, 1st Ecole Nationale Superievre de L'Aeronautique, Paris, France, September 28, 29, 1964, Proceedings.

Cerni, R. H. and L. E. Foster. Instrumentation for Engineering Measurement. New York: John Wiley and Sons, Inc., 1962.

Considine, Douglas M. Industrial Weighing. New York: Reinhold Publishing Corporation, 1948.

Cook, Nathan H. and Ernest Rabinowicz. Physical Measurement and Analysis. Reading, Massachusetts: Addison-Wesley Publishing Company, 1963.

Curry, Truman M. "A Method of Finding the Equations of Calibration Curves Typical of a Multi-Component Strain Gage Type Balance," A paper prepared at NASA Force Measurements Laboratory, Langley, Virginia, July, 1951. (Mimeographed).

Everett, Harold V. "Calibration of Skin Friction Balance Discs for Pressure Gradient." DRL 426, August 1958. Austin, Texas: Defense Research Laboratory. The University of Texas.

Guarino, J. F. "Calibration and Evaluation of Multicomponent Strain-Gage Balances," A paper prepared for presentation to the NASA interlaboratory force measurements group meeting held at J. P. L. on April 16 and 17, 1964. (Mimeographed).

Henderson, Karl C. "A Control System for the Measurement of Multi-Component, Micro-forces on a Wind Tunnel Model." MS Thesis. Charlottesville, Virginia: University of Virginia, 1966.

Hicks, David A. "Design and Development of a Gas-Supported Hydrostatic Thrust Bearing." MS Thesis. Charlottesville, Virginia: University of Virginia, 1965.

Hudson, Ralph G. The Engineers' Manual. New York: John Wiley and Sons, Inc., 1962.

Lashof, T. W. and L. B. Macurdy. "Precision Laboratory Standards of Mass and Laboratory Weights." Circular 547, Section 1. United States National Bureau of Standards, Washington, D. C. August 20, 1954.

Lion, Kurt S. Instrumentation in Scientific Research. New York:

McGraw-Hill Book Company, Inc., 1959.

Macurdy, L. B. "Performance Tests for Balances." Instruments and Control Systems, Vol. 38, Number 9, September 1965. pp. 127-133.

DISTRIBUTION LIST

Copy No.	
1 - 10	Office of Grants and Research Contracts Code CD National Aeronautics and Space Administration Washington, D. C. 20546
11	Miss Winnie M. Morgan Code SC National Aeronautics and Space Administration Washington, D. C. 20546
12	James G. Fowke Mail Stop 235, Building 1230 National Aeronautics and Space Administration Langley Field, Virginia
13	James W. Moore
14	E. S. McVey
15	W. Brown
16	RLES Files